Response to Reviewer and Short Comments:

We thank the Editor (Dr. Martin De Kauwe), Professor Luis Guanter, the Anonymous Reviewer, and Mr. Paolo Tasseron for their time and constructive comments on our manuscript.

Editor Comments:

If I could make one suggestion, which likely reflects my personal world bias. I felt like more could be done to provide a mechanistic interpretation of the double peak. For example, why would photosynthetic capacity drop and then peak again? One interpretation is differences in PAR, although I see little evidence from your Fig 6? Another is more physiological, is it a response to increasing moisture stress? You could conceivably show this by examining timeseries of air temperature, VPD (if you have it from nearby) and perhaps a climatic water deficit (e.g. PPT-PET)? Or at least, show something about precipitation that might correspond with this double peak. Currently, you show an accumulated PPT, which I don't think shows a mechanistic explanation.

Respectfully, we feel like we have provided a mechanistic interpretation of the double peak. Photosynthetic capacity has a unimodal response for the grassland+chaparral+oak savanna regions. Photosynthetic capacity also has a unimodal response for evergreen forests.

- **Peak 1 (April):** grassland + chaparral + oak savanna
- **Peak 2 (June):** evergreen forests

The processes driving these two peaks are distinct, but we then find a bimodal seasonal cycle when we look at the statewide mean because we see these two peaks. We then go on to discuss several ecophysiological reasons why this could manifest itself in a statewide double peak feature in Section 5. Finally, Section 6 (the EOF/PC analysis) further corroborates this finding by demonstrating that distinct regions in California drive the two peaks.

Page 1, Line 12: *"The double peak in the seasonality of California's photosynthesis is due to two processes that are out of phase: grasses, chaparral, and oak savanna ecosystems show an April maximum while evergreen forests peak in June."*

Page 17, Line 18: *"Several ecophysiological reasons could also explain the SIF detection of a double peak feature, whereas MODIS vegetation indices do not. Nearly 11% of the state of California consists of the California oak savanna (many in the foothills of coastal mountains and the Sierras; Tyler et al., 2006). Over the course of the season, these ecosystems operate as an evergreen ecosystem, whereby understory grass is photosynthetically active during the winter months, while trees (primarily oak species) reach extremely high values of maximum carboxylation capacity (V_{cmax}) during the spring when water is plentiful, and then retain their leaves throughout the summer in a highly photoprotective state (i.e., US-Ton; Xu and Baldocchi, 2003). Spatially, we observe increased SIF values in oak savanna as well as chaparral ecosystems (also present on coastal and Sierra foothills) in the early spring when available soil moisture is at a maximum*

(Xu and Baldocchi, 2004a; Xu et al., 2004). As these ecosystems enter the hot, dry summers, increases in sustained non-photochemical quenching and decreases in photochemistry result in decreased fluorescence, while still appearing "green" to MODIS vegetation indices. Meanwhile, snow is melting rapidly at higher elevations, making water available for many of the needleleaf evergreen species in the Sierras and Coastal ranges, then the water resources become depleted and temperatures cool prompting these evergreen species to go back into a photoprotective state, resulting in a short photosynthetically active growing season that has been shown to be more well characterized by SIF from GOME-2 than MODIS NDVI and EVI (Zuromski et al., 2018)."

Page 18, Line 27: *"The second EOF (Fig. 9b) represents the double peak in the timing of California's photosynthesis. This EOF combines the signal from the grasslands (positive phase of EOF 2) and the evergreen forests (negative phase of EOF 2). We find EOF 2 to be positively correlated with the grassland fraction from the CropScape database (r = 0.55) and negatively correlated with the evergreen forests (r = -0.36). There is also a negative correlation with the rice fields (r = -0.32). The associated principle component serves to amplify the seasonal cycle from EOF 1 in grasslands during April and amplify the forest peak in June. This is because the red region (grasslands) in Fig. 9b will contribute a positive anomaly in April and a negative anomaly in June. Conversely, the blue region (evergreen forests and rice) will contribute a negative anomaly in April and a positive anomaly in June."*

Regarding the NIRv x PAR point raised by Professor Guanter, I think that even if the authors are not going to show such a plot (for the reasons outlined), it would be very worthwhile adding some discussion text on this point.

See response to Comment #1 from Professor Guanter. We have also added the following text to the main text and a paragraph in the supplement.

Page 17, Line 31: *"Future work comparing SIF and MODIS indices with measured PAR at AmeriFlux sites would be useful in further evaluating the role of radiation and physiology in the double peak feature."*

Supplemental Section S1: *"The two peaks in the California photosynthesis seasonal cycle coincide with a slight decline in PAR inferred from ERA Interim, a time when the MODIS vegetation indices (e.g., NIR_V) remain nearly constant. If part of the difference between the SIF seasonal cycle and NIR_V seasonal cycle is indeed due to a clear sky bias as we mention, then comparing SIF with $NIR_V \times PAR$ would be the more appropriate comparison. However, the all-sky PAR dataset used in our work (ERA Interim) has a known issue that makes it unreliable (see known issue number 2: "https://confluence.ecmwf.int/display/CKB/ERA-Interim+known+issues"). The clear sky PAR from ERA Interim is reliable and, as such, we have applied a correction to the statewide PAR based on the reliable clear sky PAR but we are hesitant to draw any conclusions using this scaling at finer scales. All this is to say, the PAR data presented in main text Figure 6 is illustrative of potential reductions in PAR during May when there is a difference in the seasonal cycles from SIF and NIR_V, but we are wary of using it to directly scale NIR_V and/or compare with SIF. Further study of SIF and NIR_V in other regions is obviously needed."*

Reviewer #1 (Professor Luis Guanter) Comments:

The manuscript is very well written and presented, methods and data are innovative and the results are interesting, so I recommend it for publication in Biogeosciences. Before that, however, I would appreciate if the authors could address the following two points in their revision of the manuscript:

We thank Professor Guanter for his feedback and comments on the work.

General Comments

1.) Double peak, PAR and/or physiology? The authors acknowledge that the different seasonality in SIF and vegetation indices may be due to a clear-sky bias in the vegetation indices, but also claim that *"SIF can detect the downregulation of photosynthesis even when plants appear green"*, which seems to hint that it is not only the reaction to solar irradiance which makes SIF to show the double-peaked seasonality. To substantiate this claim, it would be interesting to see a plot of $NIR_v \times PAR_{ground}$ (with PAR_{ground} the at-surface PAR for all-sky conditions), and evaluate to what extent its seasonality resembles that of SIF. The difference between SIF and $NIR_v \times PAR$ could be attributed to physiological effects captured by SIF.

The line *"SIF can detect the downregulation of photosynthesis even when plants appear green"* was based on inferences from previous work, not inferred here. The abstract has been amended to highlight this.

Page 1, Line 9: *"The different seasonality in the vegetation indices may be due to a clear-sky bias in the vegetation indices, whereas previous work has shown SIF to have a low sensitivity to clouds and to detect the downregulation of photosynthesis even when plants appear green."*

We appreciate the suggestion from Professor Guanter to show $NIR_v \times PAR$, however there are some caveats with the available PAR data that make such a comparison unreliable. Specifically, there are known issues with the all-sky PAR data from ERA Interim: "https://confluence.ecmwf.int/display/CKB/ERA-Interim+known+issues" (see known issue number 2). The clear sky PAR from ERA Interim is reliable and we have applied a correction to the statewide PAR based on the reliable clear sky PAR but we are hesitant to draw any conclusions using this scaling at finer scales. In a similar vein, the Badgely *et al.*, GBC (2019) paper found that $NIR_v \times PAR$ worked well for predicting GPP at FLUXNET sites if they used measured PAR, but using global PAR datasets actually yielded worse estimates than if they did not include PAR as a predictor (personal communication with co-first author Lee Anderegg, UC Berkeley). This is because the global PAR datasets are poor. All this is to say, the PAR presented in Figure 6 is illustrative of potential reductions in PAR during May, but we are wary of using it to directly scale NIR_v and/or compare with SIF. Further study of SIF and NIR_v in other regions is obviously needed.

Page 17, Line 31: *"Future work comparing SIF and MODIS indices with measured PAR at AmeriFlux sites would be useful in further evaluating the role of radiation and physiology in the double peak feature."*

Supplemental Section S1: *"The two peaks in the California photosynthesis seasonal cycle coincide with a slight decline in PAR inferred from ERA Interim, a time when the MODIS vegetation indices (e.g., NIR_v) remain nearly constant. If part of the difference between the SIF seasonal cycle and NIR_v seasonal cycle is indeed due to a clear sky bias as we mention, then comparing SIF with NIR_v×PAR would be the more appropriate comparison. However, the all-sky PAR dataset used in our work (ERA Interim) has a known issue that makes it unreliable (see known issue number 2: "https://confluence.ecmwf.int/display/CKB/ERA-Interim+known+issues"). The clear sky PAR from ERA Interim is reliable and, as such, we have applied a correction to the statewide PAR based on the reliable clear sky PAR but we are hesitant to draw any conclusions using this scaling at finer scales. All this is to say, the PAR data presented in main text Figure 6 is illustrative of potential reductions in PAR during May when there is a difference in the seasonal cycles from SIF and NIR_v, but we are wary of using it to directly scale NIR_v and/or compare with SIF. Further study of SIF and NIR_v in other regions is obviously needed."*

2.) GPP scaling - The authors scale SIF to GPP as GPP*=18.5×SIF. However, I think we know better. There have been a number of papers in the last years showing that factors such as a canopy structure, photosynthetic pathway or observation geometry affect the SIF-GPP relationship making the use of a global scaling factor to be questionable. On the other hand, this study is based on the analysis of time series and no quantification of GPP is performed, so I don't see why the authors need to scale SIF to GPP values. I would therefore recommend the authors to simply use SIF rather than both SIF and GPP* in the analysis (Figs. 6 to 8).

Our reasoning for showing GPP* is to remind the reader of the major motivation for the use of SIF: to study carbon uptake. We acknowledge the shortcomings of our SIF-GPP relationship (i.e., the lack of eddy flux sites in important ecosystems) and put an asterisk on our GPP variable to emphasize that. We feel that his is a fair representation of the caveats while also highlighting the ultimate aim of work using SIF.

Page 13, Line 23: *"To reiterate, there is a clear correspondence between the observed SIF and GPP estimated for the different AmeriFlux sites (see Fig. 5) but we have a limited number of AmeriFlux sites in California that do not cover all ecosystems. As such, we do not report GPP here and have included an asterisk to highlight the caveats with the relationship presented here. Future work to obtain a more robust SIF-GPP relationship covering more ecosystems is warranted."*

Specific Comments

1.) p1, L3: "oversampling and downscaling" –> simply "downscaling" would probably be more clear for most of the readers.

We agree, updated.

2.) p2, L3: "more direct methods" than what methods?

Thanks for catching this. Updated to the following:

Page 2, Line 3: *"As such, methods of inferring..."*

3.) p2, L24: Several SIF downscaling methods have been published in the last years which are actually not based on machine learning nor intended to produce spatially-continuous SIF data sets from OCO-2 SIF retrievals. In particular, the method by Duveiller et al. to downscale GOME-2 SIF to 0.05° (last implementation here https://www.earth-syst-sci-data-discuss.net/essd-2019-121/) could also be adapted to TROPOMI. Please, discuss pros and cons of the oversampling/downscaling method presented in this manuscript with respect to that by Duveiller et al. and any other comparable downscaling method.

We appreciate Professor Guanter pointing out the Duveiller paper, however it is still under review at ESSDD and we prefer to cite final published papers in case there are changes during the review process. Additionally, the next line in our manuscript points readers to the review paper from Mohammed et al. (2019), a review article that is 39 pages long.

Page 2, Line 25: *"Mohammed et al. (2019) presents a detailed review of different remote sensing techniques for retrieving SIF from space-borne measurements."*

4.) p4, L10: "near-infrared and shortwave infrared".

Thank you for catching this, updated.

5.) p4, L19: "The TROPOMI SIF retrieval uses..." I don't think the average reader will understand this sentence without any further introduction to PCA-based SIF retrievals.

This line was included based on feedback from Professor Dennis Baldocchi (UC Berkeley; he provided feedback on an earlier version of the manuscript). He requested more details on the remote sensing and retrieval this was our balance between brevity and an exhaustive description: providing a few important points to those who work on SIF retrievals with references for interested readers to follow.

6.) p4, L 25: I can't find any information on cloud filtering, so I assume that the authors are simply not applying any. Please, discuss this here, e.g. whether no cloud filtering could/should applied globally when using SIF as a proxy for GPP (which would be somewhat scary...).

We use the same cloud filtering as Köhler *et al*. (2018). We filter pixels with VIIRS cloud fractions larger than 0.8. Text is updated as follows:

Page 4, Line 17: *"Köhler et al. (2018) filtered out pixels with cloud fractions larger than 80% based on VIIRS observations; we use this same cloud filtering here."*

7.) Fig 8. Panel C?

The updated manuscript now includes a Panel C showing the difference between fall 2019 and fall 2018.

Reviewer #2 Comments:

This work is highly interesting and its the main contribution to the scientific community is twofold: a) they introduce novel methods of oversampling and downscaling to the SIF community which offers the exciting opportunity to analyse SIF data at unprecedented spatial resolution. They also raise awareness of possible prominent retrieval biases related to bright surfaces. b) The different dynamics between canopy greenness and photosynthetic activity and the resulting benefits of SIF in general, and of TROPOMI SIF in particular, to track GPP dynamics.

However, I have two major concerns regarding the second point and main message of the paper which in my opinion are necessary to address before a publication in Biogeosciences:

We thank the Reviewer for their detailed feedback and comments on the work.

General Comments

1.) First, it is not fully clear from the work description if the comparison between greenness and SIF is meaningful: Have any filters been applied to either tower measurements, SIF or the MODIS data to remove low quality data? Also, the authors mention a clear-sky bias of the reflectance measurements as a possible explanation for the different dynamics. This implies to me that the data of VIs and SIF have not been matched in space and time before aggregating to the spatial averages shown in Fig.6. If this was indeed the case, the time series are representative of different places and therefore not fully comparable. I would like to ask the authors to clarify and if need be, to improve on this point to corroborate the main message of the paper.

Figure 2 (the scatterplot comparison) is a direct comparison between MODIS observations at the same location on the same day. This figure serves as a one-to-one comparison of the different products and the version in the supplement is expanded to include comparison with the downscaled SIF products.

For Figure 6, we interpolate the MODIS data in time for gap-filling purposes and then compute a statewide mean. The same number of points go into the statewide mean for both SIF and MODIS but there is more gap filling for MODIS. The statewide mean SIF and VIs represent our best attempt at producing a statewide mean for the different variables. The MODIS data will have gaps that need to be filled via interpolation during cloudy scenes, leaving only clear-sky conditions to build a statewide mean. TROPOMI will observe more scenes with low-to-moderate cloud cover, thus potentially inducing a clear-sky bias in the inferred statewide seasonal cycle. So the point is that the inferred seasonal cycle is different when using SIF vs VIs and part of that difference is likely due to the lack of data in cloudy periods from MODIS.

Figure 2 Caption: *"Panels show a comparison of coincident measurements in both space and time."*

2.) Second, I see the explanation for the different dynamics in SIF and greenness as incomplete. The authors convincingly argue that the different phasing of activity between evergreen forests and grasses, chaparral, and oak savanna causes the double peak in SIF. However, a similar decomposition by land cover type (Fig.6a) is missing for the greenness indices and I strongly suggest to include this in the analysis (at least for one of the indices) in order to get an idea of where/ in which ecosystems SIF and greenness are particularly dissimilar (Fig.6c). Otherwise, a sentence like in the abstract that SIF 'can detect the downregulation of photosynthesis even when plants appear green' is not justified from the material presented in the paper. Finally, this analysis of where and when VIs and SIF disagree, could be completed by a driver analysis to understand which processes does SIF see that greenness does not and to undermine the argumentation in p.17 ll.15-28. There are features as those in May in both years, which coincide with similar dips in light and rain events, it is not clear which of these is more important for which ecosystem. There are other prominent features such as the smaller peak in September 2018 in SIF which does not seem to have an obvious relationship with either precipitation or light.

The line from the abstract was based on inferences from previous work and has been amended to indicate this. See, also, the response to Comment #1 from Professor Guanter. We have included the requested driver analysis for MODIS NIR_v as two additional supplemental figures (see below).

Page 1, Line 9: *"The different seasonality in the vegetation indices may be due to a clear-sky bias in the vegetation indices, whereas previous work has shown SIF to have a low sensitivity to clouds and to detect the downregulation of photosynthesis even when plants appear green."*

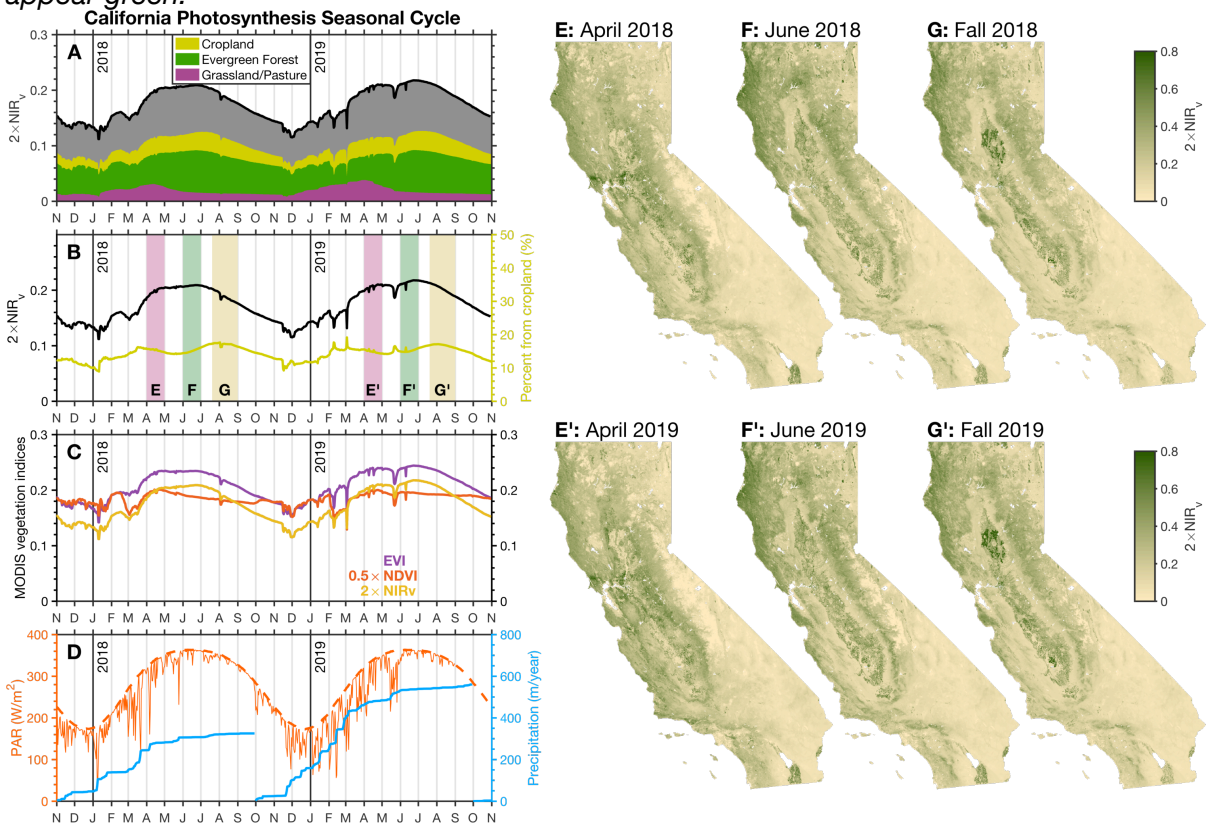

Figure S6: Same as main text Fig. 6 but for MODIS NIR_v.

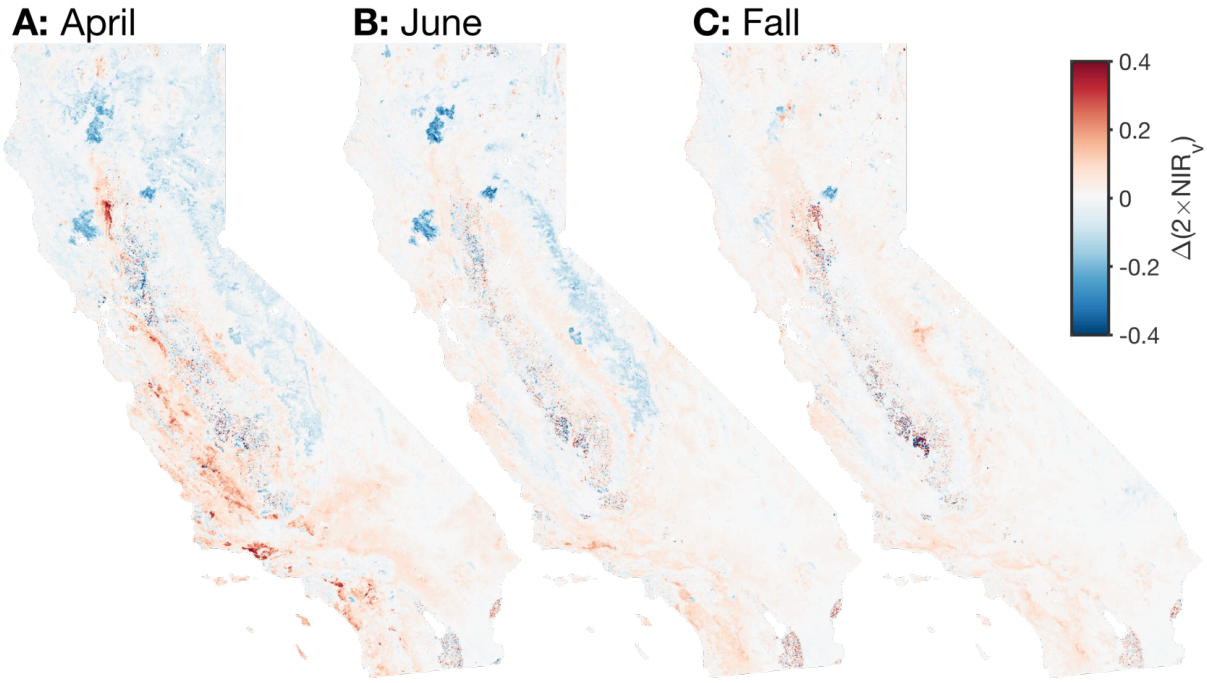

Figure S7: Same as main text Fig. 8 but for MODIS NIR_V.

Minor Comments

1.) The higher correlation between greenness and SIF at longer time scales is mentioned both in the abstract and conclusions but in the main text only in a sub-clause, and is not a main finding of your work. I see this as distracting side information as well, which does not necessarily need to be mentioned in both the abstract and the conclusions.

We disagree with the reviewer on this point. Much of the previous work comparing NIR_V and SIF was done at monthly or annual timescales and found stronger relationships (e.g., Badgely *et al.*, Science Advances 2017). As such, we do feel that it is important but there is not much additional explanation needed to understand this.

2.) Abstract: *"The different seasonality in the vegetation indices may be due to a clear- sky bias in the vegetation indices, whereas SIF has a low sensitivity to clouds and can detect the downregulation of photosynthesis even when plants appear green."* This sentence illustrates my major comment from above that the question of what drives the SIF response in the different ecosystems is not sufficiently covered by the analysis.

Updated to reflect that the latter inference was based on previous work. See response to Comment #1 from Professor Guanter and Comment #2 from Reviewer #2.

Page 1, Line 9: *"The different seasonality in the vegetation indices may be due to a clear-sky bias in the vegetation indices, whereas previous work has shown SIF to have a low sensitivity to clouds and to detect the downregulation of photosynthesis even when plants appear green."*

3.) The fact that there is a double peak in SIF but not in the VIs is mentioned twice in the conclusions.

Updated.

4.) Apart from the fact, that the scaling from SIF to GPP is not needed in this manuscript, it is rather uncommon to use the unit of mu mol/m^2/s from the tower measurements also for seasonal values as in the maps in Fig 6. gC/m^2/day is rather common.

The AmeriFlux data are provided in units of μmol/m^2/s and a number of papers use these same units. For example, the paper describing FLUXNET (Baldocchi *et al.*, 2001) uses these units for some of their figures. Magney *et al.* PNAS (2019) also used these units for some of their figures. Further, these units are useful for my own work with CO_2 flux inversions.

5.) Fig 6G' does not exist, pay attention in caption and Fig 6b.

The updated manuscript now includes Fig. 6G'.

6.) p.9 l.34: Can you really resolve daily features with an average over 14 days despite daily sampling?

We thank the review for pointing this out. We did not mean to imply that we resolve daily features, it's intended to highlight that we are **producing** our estimate every day (based on a 14-day window). Text has been updated to highlight this:

Page 9, Line 27: *"…Köhler et al. (2018) seasonal cycle is produced at weekly temporal frequency whereas we produce daily estimates using a 14-day moving window."*

7.) p.11 l.29 -p.12 l.2: To my (admittedly non-native English) ears the word 'owing' in this sentence sounds misplaced.

This is grammatically correct.

8.) Fig 6B: why is the cropland contribution stressed in this panel?

Cropland is highlighted because this is how we chose the time period for Panel G and G'.

9.) p.19 l.26: *"it seems unlikely that the grasslands and forests will exhibit opposing responses to a forcing."* It probably depends and an extended analysis as suggested above can give indications of whether this is true for California or not. There are counter examples e.g. in Flach *et al.* 2018 https://doi.org/10.5194/bg-15-6067-2018 or Walther *et al.* 2019 https://doi.org/10.1029/2018GL080535

There could certainly be a contrasting response, but it seems more likely that it falls out of the EOF requirement to compactly represent the system. From the abstract of Mohanan *et al*. (2009), a review paper on EOFs:

> "Often in the literature, EOF modes are interpreted individually, independent of other modes. In fact, it can be shown that no such attribution can generally be made. This review demonstrates that in general individual EOF modes (i) **will not correspond to individual dynamical modes**, (ii) **will not correspond to individual kinematic degrees of freedom**, (iii) **will not be statistically independent of other EOF modes**, and (iv) **will be strongly influenced by the nonlocal requirement that modes maximize variance over the entire domain**. The goal of this review is not to argue against the use of EOF analysis in meteorology and oceanography; rather, it is to demonstrate the care that must be taken in the interpretation of individual modes in order to distinguish the medium from the message."

Short Comment from Mr. Paolo Tasseron & Prof. Wouter Peters:

This review was prepared as part of graduate program course work at Wageningen University, and has been produced under supervision of Prof Wouter Peters. The review has been posted because of its good quality, and likely usefulness to the authors and editor. This review was not solicited by the journal.
…
In my opinion, the study is interesting and introduces a relevant novelty in the narrow scientific community bridging remote sensing science and photosynthesis research. However, I think three flaws are present in the current manuscript, of which I recommend some revisions before publication.

We thank Mr. Tasseron and Professor Peters for their feedback on the work. We have responded to their comments below.

General Comments

1.) To start with the first issue, on page 9 (lines 7-27) a fourteen-day moving window is used in combination with a spatial downscaling method to obtain daily estimates of SIF at a high resolution. In combination with the consequent pre-weighting of the SIF signal by the underlying vegetation fraction (MODIS NIR_v), large-scale changes in spatio-temporal patterns are conserved. On lines 20-21, the authors assume that the observed SIF from TROPOMI likely originates from more vegetated regions within that scene. However, the R^2 value of the linear correlation between SIF and NIR_v (0.52, Figure 2 on page 7) implies that a significant part of the variance in SIF cannot be explained by the underlying vegetation fraction. Besides, by using the averaged value of the 14-day moving window, a pseudo-daily average SIF value is created, rather than the actual daily value. This is fine, provided that a certain accuracy assessment is conducted. Especially because the authors mention, on page 9 lines 31-32, significant differences are found with the similar method of Köhler et

al. (2018) in which a quality control and accuracy assessment are indeed present. In addition, the downscaling (from 24.5 km^2 to 0.25 km^2) is likely to introduce inaccuracies, which requires quantification.

There is an implicit physiological argument being made here. Solar induced chlorophyll fluorescence is *inherently* a signal emitted from chlorophyll. As such, one would expect that the measured SIF signal to originate from regions within a TROPOMI scene that have more vegetation and chlorophyll.

For the second part of this comment (*"the r^2 of the linear correlation between SIF and NIR_v implies a significant part of the variance in SIF cannot be explained by underlying vegetation fraction"*), the r^2 Mr. Tasseron refers to is using two years of data over the entire state. So it implies that SIF and NIR_v do observe similar (but not identical) phenomena, making it an excellent candidate for downscaling. Regarding Mr. Tasseron's criticism of our comparison with the Köhler *et al.* (2018) paper: differences are found at fine spatial scales but large-scale patterns are consistent. Finally, we point Mr. Tasseron to our response to Comment #1 from Reviewer 2 on the temporal differences.

2.) Secondly, from page 11 onwards, the authors use a method to infer GPP from SIF, based on light-use efficiency and the probability of SIF photons escaping the canopy. Interestingly, Paul-Limognes *et al.* (2018) found that SIF was more affected by environmental conditions than GPP. Midday-depressions in SIF were linked to peak VPD values following peak photosynthetic photon flux density (PPFD). Besides, Walther *et al.* (2016) state that in evergreen needle-leaf forests, the length of the photosynthetically active period indicated by SIF is up to six weeks longer and commences a month earlier than the green biomass changing period proxied by EVI. Even though the authors used NIR_v instead of EVI to downscale SIF, the different timing could significantly alter the double peak structure. Moreover, the authors state there is a lack of GPP measurements in evergreen forests, while much of California is dominated by this vegetation type (page 13, line 17-19). In combination with the a-synchronous SIF/MODIS dynamics, this will propagate into a major bias in the scaling factor of 18.5 ± 4.9 which is inferred on page 13, line 14. Therefore, I think that the equation on page 13, line 20 ($GPP := 18.5 \bullet SIF$) should include a revised quantification of the error margins. In doing so, the authors should determine an alternative error margin whilst taking into account the fractional contribution of evergreen forests to GPP. The latter can best be inferred from a biosphere model or studies which used eddy-covariance measures in similar evergreen forests.

Regarding the first point that the use of MODIS vegetation indices could impact the double peak, it does not. The large-scale patterns are invariant to the choice of oversampling or downscaling. This can be clearly seen in the inset in the left column of Figure 4 where both the oversampling and downscaling result in the same 2018 seasonal cycle. The major features (i.e. the double peak) are also present in the Köhler *et al*. (2018) gridding for California. This is because the oversampling and downscaling conserve the SIF over a given TROPOMI pixel, so averaging to coarser spatial scales will yield an identical seasonal cycle. For the second point, see our response to Comment #2 from Professor Guanter.

The following text has been added:

Page 13, Line 23: *"To reiterate, there is a clear correspondence between the observed SIF and GPP estimated for the different AmeriFlux sites (see Fig. 5) but we have a limited number of AmeriFlux sites in California that do not cover all ecosystems. As such, we do not report GPP here and have included an asterisk to highlight the caveats with the relationship presented here. Future work to obtain a more robust SIF-GPP relationship covering more ecosystems is warranted."*

3.) Lastly, the authors successfully identify a double-peak in the seasonality of GPP. However, the number of (recent) references concerning underlying reasons for this double peak or other case studies in which a double peak is found, is unsatisfactory. References to Xu & Baldocchi (2003), Xu *et al.* (2004), Xu & Baldocci (2004) explain changes in carbon fluxes between ecosystems and vegetation types well, yet the link with SIF dynamics is lacking (Page 17, lines 15-22). Perhaps the following is a cause of the state-of-the-art novelty of this subject, but there are zero references made to any other recent papers discovering the double peak in GPP/SIF. Given the importance of this conclusion to the subject of the manuscript, I highly suggest investigating and mentioning recent existing literature explaining the double peak phenomenon. If the latter turns out to be infeasible because it is such a novelty, it is suggested to emphasize the scientific novelty in this paper. For instance, Li *et al.* (2014) imply that MODIS EVI is unsuitable for detecting a double peak in vegetated areas which usually manifest double peaks. This would strengthen the relevance as to why SIF needs to be used.

We do not reference other papers on this double peak because (to our knowledge) this is the first time it has been noted. This inference could have probably been made in earlier work (e.g., the papers we cite from the Baldocchi group) but, to our knowledge, it has not been investigated before. Satellite measurements of SIF are a fairly novel measurement (first global retrievals were made in 2011) and previous work using other satellites (e.g., GOME-2) has been limited to very coarse spatial resolutions. Our work is one of the first to get down to this spatial resolution that allows separating the processes driving this.

Given this, we chose the title of the paper to highlight the novelty of the finding. We also devoted two full sections of the text to discussing the processes driving this phenomenon.

Specific Comments

1.) In Table 1, all vegetation types have two or more study sites except for the WSA (Woody Savannas). I would like to give the authors awareness that one study site might not be representative for the entire ecosystems, especially when all other vegetation types have multiple sites.

Agreed. However, there is not much we can do in response because there simply are not additional AmeriFlux sites in California. This is, again, why we include the asterisk on GPP. We have plans to extend this analysis globally to include more sites, but the focus of this study was on California.

2.) In Figure 1, Page 3: The description mentioned that black stars show the location of six Ameriflux sites, However I can only discern three and they seem to be closely packed at this resolution.

Many of the AmeriFlux sites are in close proximity to each other. For example, the US-Tw1 US-Tw3, US-Tw4, and US-Tw5 are located on the same island in the Sacramento Delta (their longitudes differ by less than 0.01° longitude). See below for a zoomed in view of the Sacramento Delta. So there are indeed 6 AmeriFlux sites plotted, some of the stars just lie on top of each other in the Figure. This is an important point for the comparison of the wetland sites, as there is still local heterogeneity observed at these eddy flux sites that sub-grid scale.

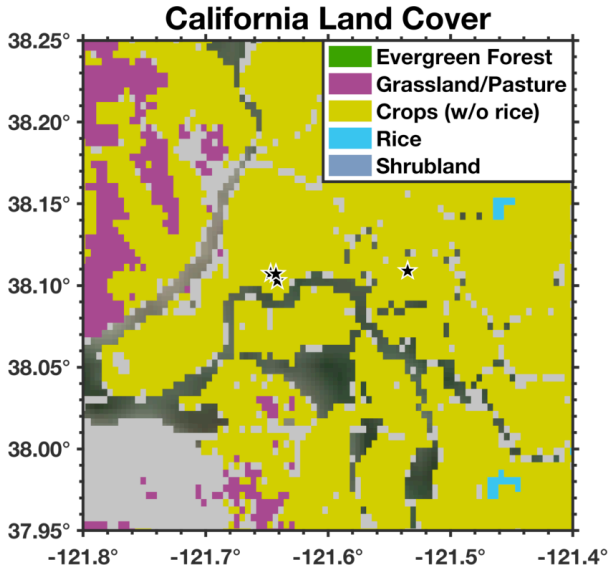

3.) In Figure 2 on page 7, the axes lack titles. This is relevant to include for the x-axes of the bottom row of graphs, as the range of the axes are different.

Axes cover the dynamic range for each product and units are included in the caption.

4.) In Figure 3 on page 8 the swath resolution is 4.0 km × 7.0 km, whereas in the text on Page 9, line 4 it is stated that this resolution is 3.5 km × 7.0 km. This should match.

The left panel is a schematic. The TROPOMI resolution at nadir is 3.5 × 7 km^2, but is larger at the edges. Supplemental Figure 1 from Köhler *et al.* (2018; see below) shows how the pixel size varies across the swath. Further, the TROPOMI team reduced the along-track integration time in August 2019 thus reducing the along-track pixel size from 7 km to 5 km. Again, this left panel referred to by Mr. Tasseron is a schematic meant to illustrate how differences in viewing geometry allow us to bisect subdivide pixels from the nominal resolution.

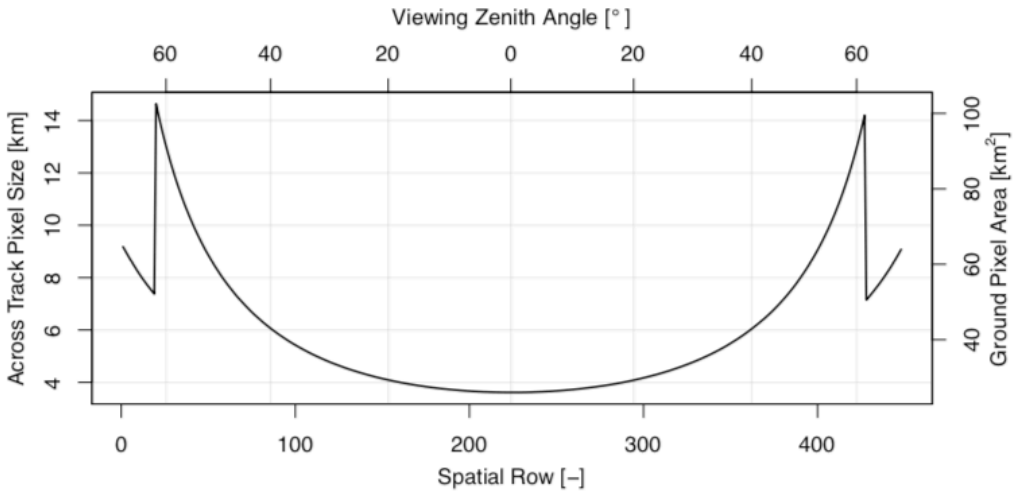

Figure S1: Across track pixel size/ground pixel area as function of spatial row/viewing zenith angle computed from soundings at the equator (same orbit as in Fig. 1).

5.) On page 9, line 19-20: perhaps it is necessary to introduce that the NIR_v was used in the pre-weighting of SIF, rather than introducing it later on Page 11, line 5.

The pre-weighting can be applied with any vegetation index, the rest of the paper simply uses NIR_v because it showed the strongest correspondence with SIF. Supplemental Figure 2 actually shows a comparison of the SIF downscaled using other MODIS vegetation indices (NDVI and EVI) as well. So we prefer to keep this expression more general here.

6.) On page 14 in the figure description, a reference to Panel G' is made, whereas this panel is not present in the accompanying figure (6).

Updated to include Panel G'.

7.) On page 16, line 8-9 it is stated that a 'reasonable consistency' is found. This should be quantified.

The figure is the quantification of the difference between the years.

8.) In the conclusion on page 20, parts of line 6-7 and line 22-23 have very similar information.

Updated.

A double peak in the seasonality of California's photosynthesis as observed from space

Alexander J. Turner[1,2,3], Philipp Köhler[4], Troy S. Magney[3,4,5], Christian Frankenberg[3,4], Inez Fung[1], and Ronald C. Cohen[1,2]

[1]Department of Earth and Planetary Sciences, University of California, Berkeley, CA, 94720, USA.
[2]College of Chemistry, University of California, Berkeley, CA, 94720, USA.
[3]Jet Propulsion Laboratory, California Institute of Technology, Pasadena, CA, 91109, USA.
[4]Division of Geological and Planetary Sciences, California Institute of Technology, Pasadena, CA, 91226, USA.
[5]Department of Plant Sciences, University of California, Davis, CA, 95616, USA.

Correspondence: Alexander J. Turner (alexjturner@berkeley.edu)

Abstract. Solar-Induced chlorophyll Fluorescence (SIF) has been shown to be a powerful proxy for photosynthesis and gross primary productivity (GPP). The recently launched TROPOspheric Monitoring Instrument (TROPOMI) features the required spectral resolution and signal-to-noise ratio to retrieve SIF from space. Here we present ~~an oversampling and~~ a downscaling method to obtain 500-m spatial resolution SIF over California. We report daily values based on a 14-day window. TROPOMI SIF data show a strong correspondence with daily GPP estimates at AmeriFlux sites across multiple ecosystems in California. We find a linear relationship between SIF and GPP that is largely invariant across ecosystems with an intercept that is not significantly different from zero. Measurements of SIF from TROPOMI agree with MODIS vegetation indices (NDVI, EVI, and NIR_V) at annual timescales but indicate different temporal dynamics at monthly and daily timescales. TROPOMI SIF data show a double peak in the seasonality of photosynthesis, a feature that is not present in the MODIS vegetation indices. The different seasonality in the vegetation indices may be due to a clear-sky bias in the vegetation indices, whereas ~~SIF has~~ previous work has shown SIF to have a low sensitivity to clouds and ~~can~~ to detect the downregulation of photosynthesis even when plants appear green. We further decompose the spatio-temporal patterns in the SIF data based on land cover. The double peak in the seasonality of California's photosynthesis is due to two processes that are out of phase: grasses, chaparral, and oak savanna ecosystems show an April maximum while evergreen forests peak in June. An empirical orthogonal function (EOF) analysis corroborates the phase offset and spatial patterns driving the double peak. The EOF analysis further indicates that two spatio-temporal patterns explain 84% of the variability in the SIF data. Results shown here are promising for obtaining global GPP at sub-kilometer spatial scales and identifying the processes driving carbon uptake.

1 Introduction

Photosynthesis is the process by which plants and other organisms use sunlight to synthesize carbon dioxide (CO_2) and water to glucose and oxygen. Accurate knowledge of gross primary productivity (GPP) through photosynthesis is crucial for understanding the land-atmosphere carbon exchange, which is one of the largest and most uncertain aspects of the global carbon

cycle (IPCC, 2013; Anav et al., 2015; USGCRP, 2018). This uncertainty in the land-atmosphere carbon exchange has led to long-standing questions regarding the magnitude of the Northern Hemispheric terrestrial carbon sink and how it has changed over the past few decades (e.g., Tans et al., 1990; Ballantyne et al., 2012; Ciais et al., 2019). As such, ~~more direct~~ methods of inferring GPP are of great interest to the scientific community.

Previous work estimating regional or global scale GPP has typically relied on either biosphere models (e.g., the early work on SiB2 from Sellers et al., 1986), used remote-sensing measurements in Monteith light use efficiency models with scalings for different ecosystems and climatic conditions (e.g., Monteith, 1972; Mahadevan et al., 2008), or attempted to back out GPP from CO_2 flux inversions (e.g., CarbonTracker from Peters et al., 2007). The advent of global remote-sensing observations of Solar-Induced chlorophyll Fluorescence (SIF) represents a breakthrough in our ability to constrain photosynthetic activity from space. This is because a number of studies have shown SIF to be a powerful proxy for photosynthesis both in laboratory environments (e.g., Baker, 2008) and at larger spatial scales (e.g., Frankenberg et al., 2011a; Parazoo et al., 2014; Yang et al., 2015, 2017; Sun et al., 2017, 2018b; Magney et al., 2019a). During the initial stage of photosynthesis, absorbed sunlight excites chlorophyll a molecules. The primary pathways for de-excitation are via photochemistry or non-photochemical quenching, the latter of which dissipates excess energy as heat when the plant does not have the capacity for photosynthesis (i.e. under stress). However, a small fraction dissipates as heat or is re-emitted as fluorescence and can be measured by remote sensing. This remote sensing retrieval is termed SIF.

The first global space-borne measurements of SIF were made by Frankenberg et al. (2011b) and Joiner et al. (2011) using observations from the Japanese GOSAT instrument (Kuze et al., 2009). Since then, SIF has been retrieved from other space-borne instruments such as: GOME-2 on the METOP-A satellite, SCIAMACHY on the ENVISAT satellite, the OCO-2 satellite, and TROPOMI on the Sentinel-5 Precursor satellite (Frankenberg et al., 2011a, b, 2012, 2014; Joiner et al., 2011, 2012, 2013, 2014, 2016; Guanter et al., 2012, 2015; Köhler et al., 2015, 2018). A number of upcoming satellite missions such as FLEX (Drusch et al., 2017) and TEMPO (Zoogman et al., 2017) will also measure SIF at higher spatial and temporal resolution. Efforts are underway to create a multi-decadal SIF record using different space-borne instruments (Parazoo et al., 2019) and a few groups have utilized machine learning techniques to create spatially continuous SIF datasets at $0.05^\circ \times 0.05^\circ$ resolution (Zhang et al., 2018; Yu et al., 2019; Li and Xiao, 2019). Mohammed et al. (2019) presents a detailed review of different remote sensing techniques for retrieving SIF from space-borne measurements.

Some work has shown SIF to be a better measure of carbon uptake than other vegetation indices that look at canopy "greenness". This is, in part, because indices like the normalized difference vegetation index (NDVI) are a measure of photosynthetic capacity (Sellers et al., 1986) whereas SIF is a measure of the photosynthetic activity and is coupled to the radiation regime. For example, Luus et al. (2017) showed that the seasonal cycle of a biosphere model driven by SIF agreed with measurements of CO_2 whereas the seasonal cycle from the model driven by the Enhanced Vegetation Index (EVI) was markedly different from the CO_2 observations. Joiner et al. (2011) showed that the seasonal cycles of SIF and EVI agree in some regions, but not others. Walther et al. (2016) showed a decoupling of the photosynthesis and greenness dynamics in boreal evergreen forests by comparing SIF and EVI to model estimates of GPP, with SIF better capturing the seasonality of both deciduous broadleaf and evergreen needleleaf forests. Again, this is likely due to SIF capturing photosynthetic activity, rather than photosynthetic

capacity. More recently, Magney et al. (2019a) demonstrated a mechanistic link between SIF and GPP over the course of a year in a winter-dormant Northern Hemisphere conifer forest, despite retaining chlorophyll through the winter. Magney et al. (2019a) highlighted the potential for new satellite measurements of SIF from TROPOMI and OCO-2 to track GPP at coarse spatial resolution (3.5×7 km^2).

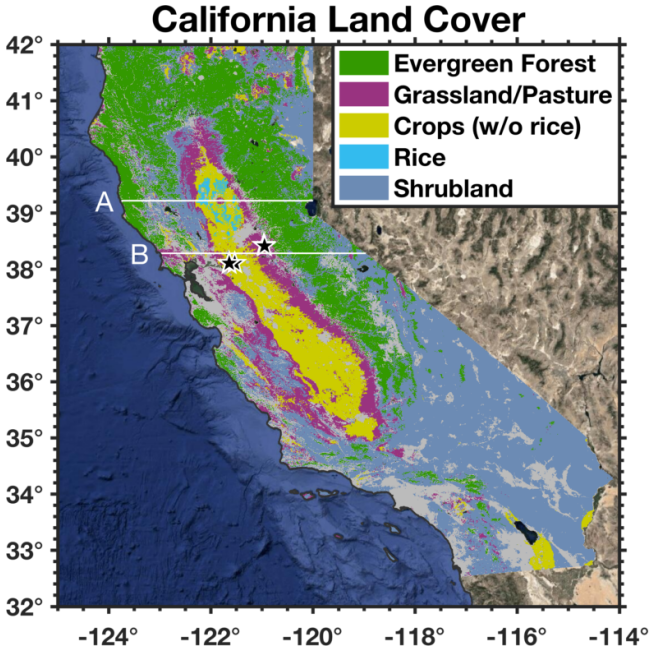

Figure 1. California land cover. Land cover in California from the 2018 USDA CropScape database (USDA, 2018). Resolution has been degraded from the native 30-m resolution to 500-m for comparison with TROPOMI data. Coloring indicates that a land type makes up more than 50% of the 500-m grid cell. White lines are the locations of two transects across California for Hovmöller diagrams: 39.218°N (Transect A), and 38.282°N (Transect B). Black stars show the location of six AmeriFlux sites: Bouldin Island (38.1090°N, 121.5350°W; US-Bi2), Tonzi Ranch (38.4316°N, 120.9660°W; US-Ton), Vaira Ranch (38.4133°N, 120.9507°W; US-Var), Twitchell Island West Pond (38.1074°N, 121.6469°W; US-Tw1), Twitchell Island East End (38.1030°N, 121.6414°W; US-Tw4), and Twitchell Island East Pond (38.1072°N, 121.6426°W; US-Tw5).

Here we present an oversampling and downscaling method to obtain daily estimates of SIF at 500-m resolution. To our knowledge, this is the highest resolution SIF dataset from satellite measurements. We then compare this down-scaled 500-m SIF data to AmeriFlux sites across the state of California to assess the relationship between SIF and GPP. We finish by decomposing California's spatio-temporal patterns of photosynthesis and carbon uptake into the dominant modes using empirical orthogonal functions (EOFs). Here we focus on California because there are a number of eddy flux towers and it encompasses a range of diverse ecosystems including: deciduous and evergreen forests, irrigated croplands, and grasslands (see Fig. 1).

2 Measurements of SIF, vegetation, and GPP

2.1 Satellite measurements of Solar-Induced chlorophyll Fluorescence (SIF) from TROPOMI

The TROPOspheric Monitoring Instrument (TROPOMI; Veefkind et al., 2012) is a nadir-viewing imaging spectrometer with bands in the UV, visible, ~~shortwave infrared, and near-infrared~~ near-infrared, and shortwave infrared aboard the Sentinel-5 Precursor satellite. The Sentinel-5 Precursor satellite was launched into low earth orbit on October 13, 2017 with an equatorial crossing time of 13:30 local solar time and a 16 day orbit cycle. TROPOMI has a wide swath (2,600 km across track) enabling near-daily global coverage. The spatial resolution of the ground pixels is 7 km along track[1] and 3.5-15 km across track (3.5 km at nadir and 15 km at the edge of the swath). Of particular relevance here is the near-infrared band (725-775 nm) that covers the far-red part of SIF emission and contains a number of solar absorption features in the solar irradiance (Fraunhofer lines), allowing for retrieval of SIF through the change in optical depth of Fraunhofer lines. Guanter et al. (2015) showed the potential for TROPOMI to retrieve SIF and Köhler et al. (2018) presented the first retrievals. Specifically, Köhler et al. (2018) used a 743-758 nm retrieval window that is devoid of atmospheric absorption features. TROPOMI has a spectral resolution of ∼0.4 nm and a signal-to-noise ratio of ∼2,500 in this retrieval window. The TROPOMI SIF retrieval uses a singular value decomposition to derive the spectral basis functions from TROPOMI data over vegetation-free areas (e.g., oceans, ice, and deserts).

One particularly attractive feature of space-borne SIF retrievals is the low sensitivity to atmospheric scattering by aerosols and clouds. Specifically, Frankenberg et al. (2012) showed that 80% of the emitted SIF could be retrieved in the presence of clouds with low-to-moderate optical thickness. As such, Köhler et al. (2018) filtered out pixels with cloud fractions larger than 80% based on VIIRS observations; we use this same cloud filtering here. This weak sensitivity to clouds is in contrast to reflectance based measures of vegetation (e.g., NDVI) that can only be made in clear-sky conditions, potentially inducing a clear-sky bias in reflectance based vegetation indices.

Here, we apply one additional bias correction to the TROPOMI retrievals that was not included in Köhler et al. (2018). We find some mostly barren regions have systematically negative SIF values, which is non-physical. This bias is thought to be related to bright surfaces and is likely due to the choice of training data for the spectral basis functions. We are investigating ways to correct this globally. In the interim, we compute a spatio-temporal bias correction $b_{i,j,k}$ (where i,j are the spatial coordinates and k is the temporal coordinate) such that the mean SIF for a given location over a 30-day moving window is always positive. That is to say,

$$b_{i,j,k} = \begin{cases} |\bar{s}_{i,j,k}|, & \bar{s}_{i,j,k} < 0 \\ 0, & 0 \leq \bar{s}_{i,j,k} \end{cases} \quad (1)$$

where $\bar{s}_{i,j,k}$ is the 1-month block average for the k^{th} day at location i,j. This still allows for negative SIF values due to variability and noise but will shift the mean SIF for a given 500-m grid cell to be positive. In practice, this bias correction is small

[1] Along track resolution increased to 5.6 km in August 2019 (http://www.tropomi.eu/mission-status).

with 78% having no bias correction at all and 89% of the grid cells having a bias correction smaller than 0.1 mW/m^2/sr/nm. The bias correction primarily impacts desert regions in Southeastern California (see Supplemental Fig. S1).

2.2 Satellite-based vegetation indices from MODIS

MODerate Resolution Imaging Spectroradiometer (MODIS) is an imaging spectrometer on NASA's Terra and Aqua satellites. Terra launched in 2000 and Aqua launched in 2002, both are in sun-synchronous orbits with 16 orbits per day. Terra and Aqua have equatorial crossing at 10:30 and 12:00 local solar time, respectively. Schaaf et al. (2002) developed the Nadir Bidirectional reflectance distribution function-Adjusted Reflectance (NBAR) dataset, hereafter referred to as the MODIS NBAR dataset. MODIS data over a 16-day period from Terra and Aqua can be combined to build a 500-m composite: MCD43A4. Here we use the MCD43A4.006 (v06) MODIS NBAR dataset to compute three MODIS vegetation indices at 500-m resolution. Specifically, we compute the normalized difference vegetation index (NDVI), enhanced vegetation index (EVI), and near-infrared reflectance of vegetation index (NIR$_\mathrm{v}$):

$$\mathrm{NDVI} = \frac{\rho_\mathrm{NIR} - \rho_\mathrm{red}}{\rho_\mathrm{NIR} + \rho_\mathrm{red}} \tag{2}$$

$$\mathrm{EVI} = G \cdot \frac{\rho_\mathrm{NIR} - \rho_\mathrm{red}}{\rho_\mathrm{NIR} + C_1\rho_\mathrm{red} - C_2\rho_\mathrm{blue} + L} \tag{3}$$

$$\mathrm{NIR_v} = \rho_\mathrm{NIR} \cdot \mathrm{NDVI} \tag{4}$$

where ρ_NIR, ρ_red, and ρ_Blue are the reflectances in their respective MODIS bands and G, C_1, C_2, and L are coefficients for the MODIS EVI algorithm ($L = 1$, $C_1 = 6$, and $C_2 = 7.5$, $G = 2.5$).

2.3 GPP estimates from AmeriFlux eddy covariance sites

AmeriFlux is a network of long-term eddy covariance sites that launched in 1996 (Baldocchi et al., 2001). These eddy covariance sites provide a direct measure of net ecosystem exchange (NEE; CO_2 fluxes) (Baldocchi et al., 1988) and can be used to evaluate both bottom-up models and satellite proxies of carbon exchange. Disentangling the CO_2 fluxes into GPP (CO_2 uptake) and total ecosystem respiration (R_eco; CO_2 released) generally requires making assumptions about the temperature dependence of the respiration which can induce biases in the GPP estimate (Reichstein et al., 2005). Nevertheless, these eddy covariance sites provide the best estimate of site level GPP across multiple ecosystems in California including: croplands, wetlands, woody savannas, and grasslands. Here we use data from 11 AmeriFlux sites across California (see Table 1) to evaluate the SIF retrievals from TROPOMI. NEE flux partitioning at these sites was performed using artificial neural networks from nighttime measurements to constrain R_eco (Hemes et al., 2019).

2.4 Comparison of TROPOMI SIF with MODIS vegetation indices

Figure 2 shows a scatterplot comparison of TROPOMI SIF and MODIS NDVI, EVI, and NIR$_\mathrm{v}$. The comparison is limited to coincident observations between March and August (MAMJJA) and excludes scenes that are predominantly barren or shrubland. A few features that immediately stand out are:

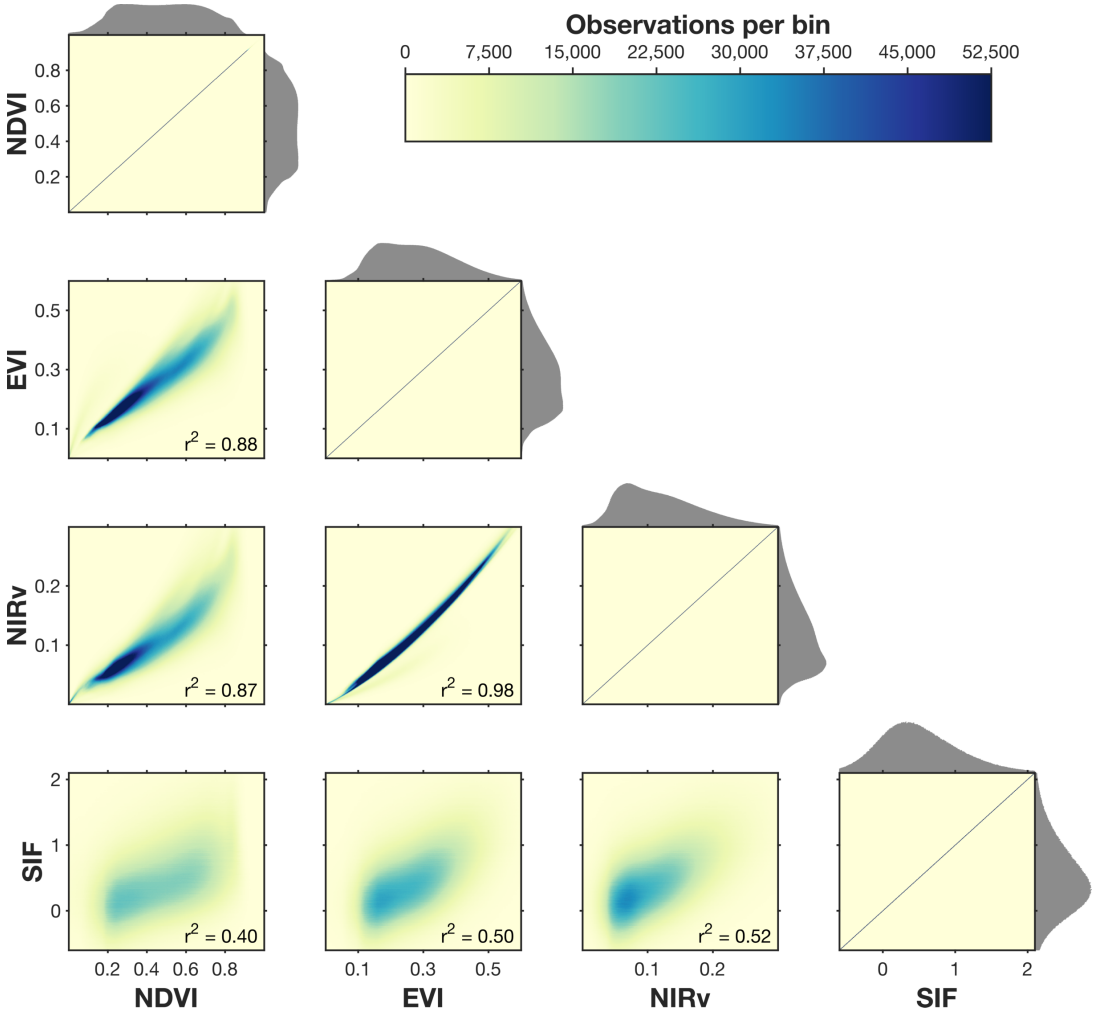

Figure 2. Comparison of MODIS vegetation indices and TROPOMI SIF from 2018-2019. Panels show a comparison of coincident measurements in both space and time of NDVI, EVI, NIR_V, and SIF. NDVI, EVI, and NIR_V use the 500-m MODIS BRDF-corrected reflectances and SIF is from TROPOMI. Shading indicates the density of points. Data is filtered to only include measurements from March through August (MAMJJA). Data is further filtered to remove scenes that are more than 85% barren or shrubland as defined by the CropScape Database. Gray histogram on the x/y-axes show the distribution of values for a given set of data. NDVI, EVI, and NIR_V are unitless and SIF has units of $mW/m^2/sr/nm$. Supplemental Fig. S2 shows the comparison including the SIF downscaled using local MODIS vegetation indices.

Table 1. AmeriFlux sites used in this study.

Site ID	Site name	Latitude (°N)	Longitude (°W)	Elevation (m a.s.l.)	Vegetation type[a]
US-Bi1	Bouldin Island Alfalfa	38.0992	121.4993	-3	CRO[b]
US-Bi2	Bouldin Island Corn	38.1090	121.5350	-5	CRO[b]
US-EDN	Eden Landing Ecological Reserve	37.6156	122.1140	1	WET[c]
US-Myb	Mayberry Wetland	38.0499	121.7650	-4	WET[c]
US-Sne	Sherman Island Restored Wetland	38.0369	121.7547	-5	GRA[d]
US-Ton	Tonzi Ranch	38.4316	120.9660	177	WSA[e]
US-Tw1	Twitchell Island West Pond	38.1074	121.6469	-9	WET[c]
US-Tw3	Twitchell Island Alfalfa	38.1159	121.6467	-9	CRO[b]
US-Tw4	Twitchell Island East End	38.1030	121.6414	-5	WET[c]
US-Tw5	Twitchell Island East Pond	38.1072	121.6426	-5	WET[c]
US-Var	Vaira Ranch	38.4133	120.9507	129	GRA[d]

[a] Vegetation classification based on the International Geosphere-Biosphere Programme (IGBP) classification scheme (Strahler et al., 1999).

[b] CRO (Croplands): Lands covered with temporary crops followed by harvest and a bare soil period (e.g., single and multiple cropping systems). Note that perennial woody crops will be classified as the appropriate forest or shrub land cover type.

[c] WET (Permanent Wetlands): Lands with a permanent mixture of water and herbaceous or woody vegetation that cover extensive areas. The vegetation can be present in either salt, brackish, or fresh water.

[d] GRA (Grasslands): Lands with herbaceous types of cover. Tree and shrub cover is less than 10%.

[e] WSA (Woody Savannas): Lands with herbaceous and other understory systems, and with forest canopy cover between 30-60%. The forest cover height exceeds 2 meters.

1. The strong correspondence between EVI and NIR_v. We find a nearly linear relationship between these two indices ($r^2 = 0.98$).

2. All three MODIS indices are well correlated with eachother ($r^2 > 0.85$). We do observe a weakly non-linear relationship between NIR_v and EVI or NDVI (see the curvature in the NIR_v row).

3. The weaker relationship between SIF and the vegetation indices. Previous work has argued that NIR_v is strongly correlated with SIF (Badgley et al., 2017) and provides a new independent approach for estimating GPP (Badgley et al., 2019).

Of the three vegetation indices examined here, we find the strongest relationship between NIR_v and SIF, but it only explains half of the variability on daily timescales ($r^2 = 0.52$). The agreement improves at coarser temporal scales (annual r^2 = 0.83–

0.84 and monthly r^2 = 0.59±0.23). It is important to note that the native spatial resolution of the TROPOMI observations are 3.5-km across-track at nadir, whereas the MODIS observations are 500-m across-track at nadir. As such, we are using all MODIS observations within a single TROPOMI scene. Comparison of four methods of downscaling SIF with NIR_v yield coefficients of determination of $r^2 = 0.52 - 0.64$; see Fig. S2).

3 Oversampling and spatial-downscaling of TROPOMI data

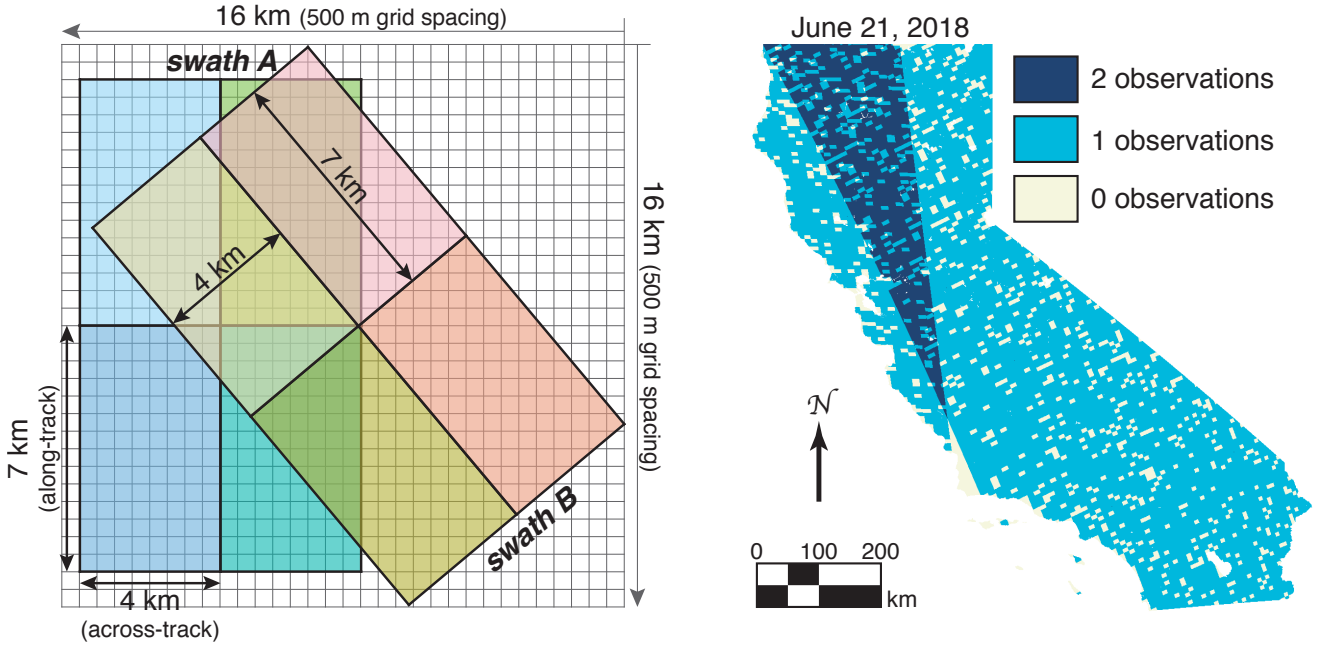

Figure 3. Oversampling schematic. Left panel shows the schematic for our oversampling. Gray grid has a grid spacing of 500 m (equivalent to the spatial resolution of the MODIS MCD43A4 product). TROPOMI ground pixels are 7 km along-track and vary from 3.5 km (at nadir) to 15 km off swath edge) across-track. Schematic shows the spatial extent of eight hypothetical TROPOMI scenes from two swaths at 7×4 km^2, individual TROPOMI scenes are a different color. Swath B is rotated 40° relative to swath A, resulting in overlapping pixels. Right panel shows the number of successful retrievals on June 21, 2018 over California plotted on a 500-m grid.

As mentioned above, the nominal spatial resolution of the ground pixels from TROPOMI are 3.5×7 km^2 at nadir. However, the wide swath from TROPOMI (2600 km across-track) often results in multiple observations per day (see right panel of Fig. 3). Additionally, the orientation of these swaths differ over the 16-day orbit cycle allowing us to infer higher spatial resolution than the nominal spatial resolution. This idea has been widely used with the space-borne OMI instrument that preceded TROPOMI (see Sun et al., 2018a, and references therein for a discussion of oversampling with OMI observations). However, the spatial resolution of TROPOMI is a factor of 15 finer than OMI (3.5×7 km^2 for TROPOMI and 14×26 km^2 for

OMI, both at nadir). Oversampling with OMI often required years of observations (e.g., Zhu et al., 2014). The wide swath and ~~high spatial~~ dense spatial coverage of TROPOMI allow us to perform biweekly oversampling.

Fig. 3 shows a schematic of how the oversampling is performed. The left panel shows two hypothetical swaths from TROPOMI overlaid on a 500-m grid (same spatial resolution as the MODIS NBAR dataset). Areas where the swaths overlap allow ~~for~~ us to partition the information down to a finer spatial scale. For example, the yellow pixel in swath B overlaps with all four pixels from swath A. As such, the signal from that pixel in swath B can be sub-divided to finer spatial scales. Each unique shade of color would correspond to unique information in the left panel of Fig. 3. The right panel of Fig. 3 shows the sampling density of TROPOMI over California on a single day in June 2018, the dark blue region indicates where two TROPOMI swaths overlapped that day.

We find that, on average, each 500-m grid cell is within the bounds of ~0.6 TROPOMI scenes with a successful retrieval per day. By using biweekly oversampling (a moving 14-day window) we obtain approximately 8 different swath orientations over a 14-day period for the oversampling. These 8 swath orientations allow us to further refine our grid to following the schematic shown in Figure 3. It also means that the daily values presented here are representative of 14-day moving averages (centered about that day).

We can take the oversampling a step further by pre-weighting the SIF signal in a TROPOMI scene by the underlying vegetation fraction, we refer to this as "downscaling". That is to say, we assume the observed SIF from TROPOMI in a given scene likely originates from more vegetated regions within that scene. Here we use a relative weighting for this downscaling:

$$s_{i,j} = s^{\star} \frac{v_{i,j}}{\bar{v}} \tag{5}$$

where $s^{\star}$ is the retrieved SIF from TROPOMI for a single scene, $s_{i,j}$ is the SIF spatially downscaled to 500-m, $v_{i,j}$ are the vegetation indices from MODIS that fall within the bounds of a single scene from TROPOMI (i.e., the gray boxes within a TROPOMI box in the left panel of Fig. 3), and $\bar{v}$ is the mean vegetation index over a given TROPOMI scene. Using Eq. 5 with $\mathbf{v} = [1, \ldots, 1]$ returns the unweighted oversampling result. Following this, $s_{\mathrm{i,j}}$ will naturally revert to oversampling in regions with homogeneous vegetation (as inferred by MODIS).

Figure 4 shows the 2018 annual mean SIF from TROPOMI from Köhler et al. (2018) at $0.05^{\circ} \times 0.05^{\circ}$ spatial resolution and California's seasonal cycle at weekly temporal resolution (non-bias corrected). The middle and bottom rows of Figure 4 show the 2018 annual mean SIF and seasonal cycle using oversampling and spatially downscaled with $\mathrm{NIR_v}$ from MODIS. All three show consistent large-scale spatial patterns. We do, however, find significant differences between the results from Köhler et al. (2018) and the oversampling or downscaling method over the San Francisco Bay Area where the complex topography induces numerical artifacts such as high SIF values over water. We also point out that the Köhler et al. (2018) seasonal cycle is produced at weekly temporal ~~resolution whereas we obtain daily temporal resolution because of the~~ frequency whereas we produce daily estimates using a 14-day moving window. The oversampling and downscaling methods both yield consistent large-scale patterns and seasonal cycles (left panels in Fig. 4). The main impact of the MODIS-based local downscaling is a sharpening effect. This can be seen in the right column of Fig. 4. Importantly, the gradients observed in the oversampled SIF are also present in the downscaled SIF. The choice of MODIS vegetation index to use in the downscaling makes little difference

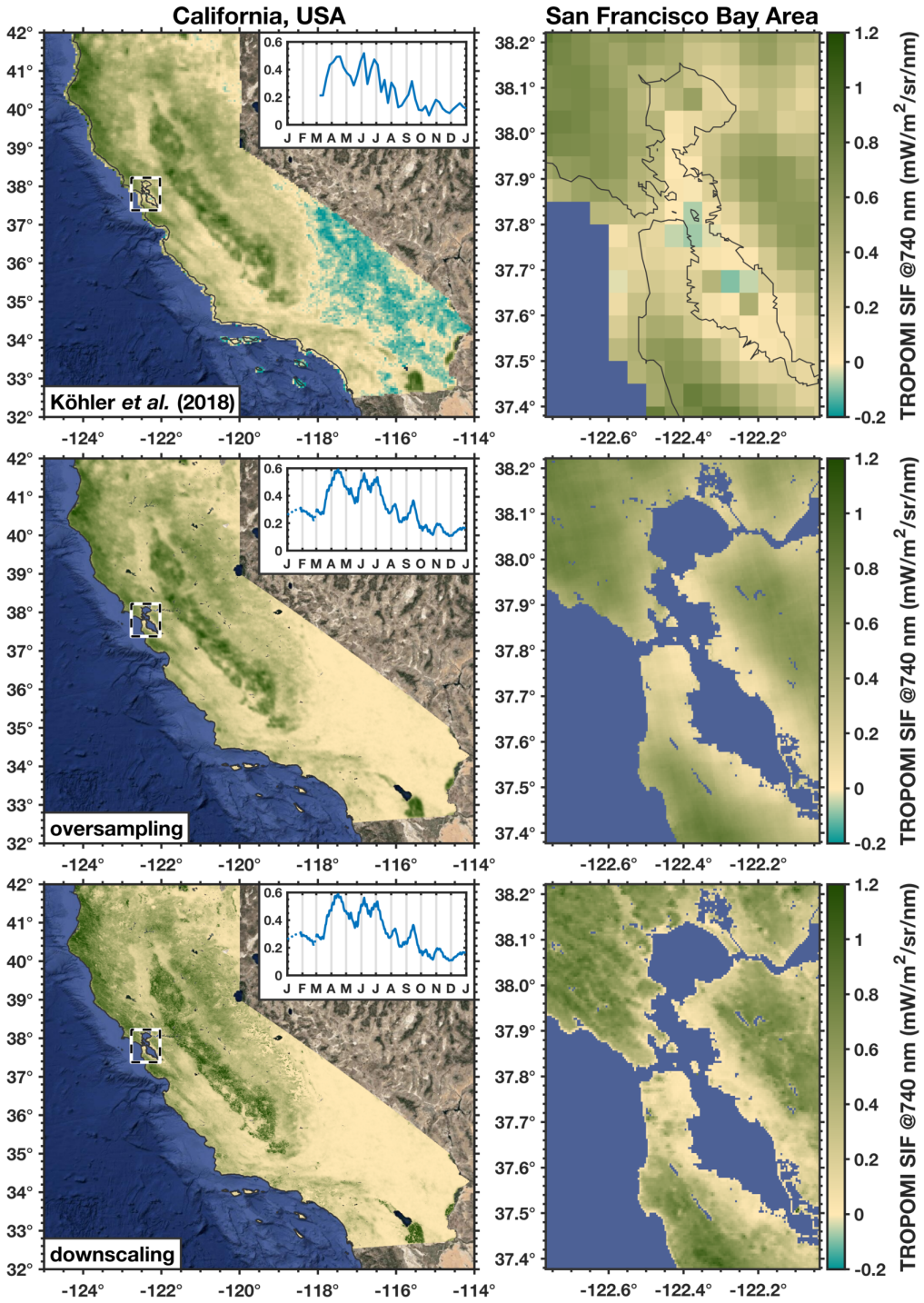

Figure 4. 2018 annual mean photosynthesis. Top row shows the 2018 annual mean TROPOMI SIF from Köhler et al. (2018) and inset shows the seasonal cycle ($0.05^\circ \times 0.05^\circ$ spatial resolution and weekly temporal resolution, respectively). Middle row uses the same TROPOMI SIF data but but oversampled to 500-m spatial resolution and daily temporal resolution. Bottom row uses an NIR_V-weighted local downscaling to 500-m spatial resolution. Left column shows all of California, USA and right column shows the San Francisco Bay Area in detail. Dashed black line in the left column indicates the domain of the right column.

as the r^2 between the different downscaled SIF products range from 0.99-1.00 (see Fig. S2), hereafter we use SIF downscaled with NIR_v because, of the three vegetation indices, NIR_v showed the strongest correlation to SIF (see Fig. 2). Again, we stress that the large-scale spatio-temporal patterns are conserved between the oversampling and downscaling methods and the nuanced difference in processing allow for analysis at much finer spatio-temporal scales. That is to say that we are not inducing large-scale changes in the spatio-temporal patterns with these different methods of processing, those are robustly driven by the underlying SIF retrievals.

4 Inferring GPP from SIF

Previous work has shown strong empirical relationships between SIF and GPP at coarse spatial scales (e.g., Walther et al., 2016; Jeong et al., 2017; Parazoo et al., 2018; Zuromski et al., 2018; Sun et al., 2018b). Magney et al. (2019a) recently extended this SIF-GPP relationship by showing, in a conifer forest, how both SIF and GPP are regulated by seasonal changes in photoprotective pigments and how SIF is directly related to needle physiology.

Lee et al. (2013), Guanter et al. (2014), and Sun et al. (2017) have previously argued for a linear relationship between SIF and GPP, this follows from a simple relational analysis. From Monteith theory (Monteith, 1972) we can write:

$$\mathrm{GPP} = \Phi_{\mathrm{CO_2}} \alpha I \tag{6}$$

where $\Phi_{\mathrm{CO_2}}$ is the light use efficiency of CO_2 assimilation, I is the photosynthetically active radiation (PAR), and α is the fractional absorbance of PAR. An analogous expression can be written for SIF (Lee et al., 2013):

$$\mathrm{SIF} = \Phi_F \alpha \beta I \tag{7}$$

where Φ_F is the the light-use efficiency of SIF and β is the probability of SIF photons escaping the canopy. Rearranging yields:

$$\mathrm{GPP} = \frac{\Phi_{\mathrm{CO_2}}}{\beta \Phi_{\mathrm{F}}} \mathrm{SIF}. \tag{8}$$

From Eq. 8 we can see that GPP should be proportional to SIF. However, there are likely differences in $\Phi_{\mathrm{CO_2}}/(\beta\Phi_F)$ between ecosystems. Notably, Yang et al. (2018) argued that SIF is more strongly correlated with the absorbed PAR (αI) than with GPP at sub-daily timescales, which implicitly points to non-linearities in $\Phi_{\mathrm{CO_2}}/(\beta\Phi_F)$. β will be a function of the canopy structure and likely differs between ecosystems, although some studies have argued that reflectance measurements could be used to infer β (Yang and van der Tol, 2018; Zeng et al., 2019). Additionally, the ratio of $\Phi_{\mathrm{CO_2}}$ to Φ_F will likely be ecosystem specific due to, for example, differences in photosynthetic pathways (C3 versus C4 plants; Liu et al., 2017). A number of studies have found the relationship between chlorophyll fluorescence and GPP to be non-linear at the leaf-scale (e.g., Magney et al., 2017, 2019b), owing the increased linearity at the canopy scale to averaging SIF and GPP over many different leaf angles exposed to highly heterogenous light environments.

Figure 5 compares the TROPOMI SIF retrievals to observations from AmeriFlux sites across California (see Table 1 and Fig. 1 for the locations). The gray dots in Fig. 5 are all of the AmeriFlux GPP estimates and the black dots are those between

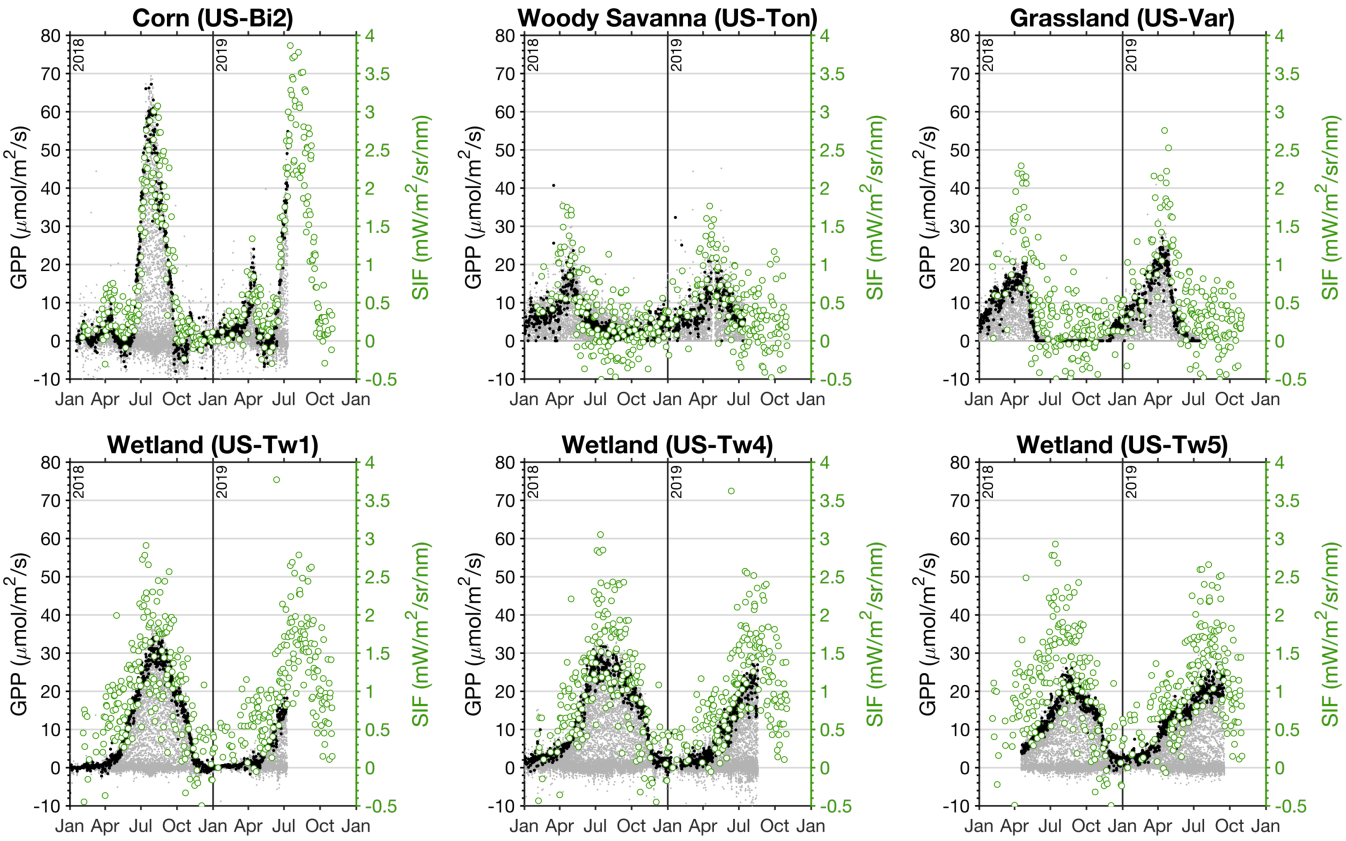

Figure 5. AmeriFlux GPP and TROPOMI SIF at six sites in California. Left axes (black) show GPP from AmeriFlux and right axes (green) show SIF from TROPOMI that have been downscaled with NIR_V. Light gray dots show all of the GPP measurements from the AmeriFlux site and black dots indicate GPP measurements between 13:00-14:00 PST (TROPOMI equatorial overpass is 13:30 local solar time). Green circles show the TROPOMI SIF observations at the AmeriFlux sites after applying the scene-specific relative weighting from the MODIS NIR_V. AmeriFlux sites used are: Bouldin Island (US-Bi2; 38.1090°N, 121.5350°W), Tonzi Ranch (US-Ton; 38.4316°N, 120.9660°W), Vaira Ranch (US-Var; 38.4133°N, 120.9507°W), Twitchell Island West Pond (US-Tw1; 38.1074°N, 121.6469°W), Twitchell Island East End (US-Tw4; 38.1030°N, 121.6414°W), and Twitchell Island East Pond (US-Twt; 38.1072°N, 121.6426°W). CO_2 flux measurements and comparisons for other sites listed in Table 1 are shown in Supplemental Figs. S3 and S4.

13:00-14:00 PST, similar to the TROPOMI overpass time (equatorial overpass time is 13:30 local solar time at nadir). This overpass time is fortuitous in that it generally coincides with the daily maximum in GPP at the AmeriFlux sites. The green dots are the actual TROPOMI SIF retrievals at that location that have the scene-specific relative weighting from the MODIS NIR_V (Eq. 5). No temporal smoothing has been applied in Fig. 5. We find a strong correspondence between SIF and GPP across four different ecosystems. The top left panel shows that SIF clearly captures the onset of photosynthesis as well as the punctuated seasonal cycle of GPP in a corn field (US-Bi2) with r^2 = 0.79. We also observe the gradual increase in GPP and abrupt decline at a woody savanna site (US-Ton) and grassland site (US-Var) with r^2 = 0.40 and r^2 = 0.59, respectively. The relatively high variability in SIF at US-Ton and US-Var from July to December (1-σ spread of 0.33 mW/m^2/sr/nm) contrasts the low variability during the dormant period at US-Bi2 and is likely associated with bright surfaces (implying a higher retrieval uncertainty), quantifying the upper range of anticipatable noise. The bottom row of Fig. 5 shows a comparison of TROPOMI SIF with GPP from three different wetland sites on Twitchell Island in the Sacramento-San Joaquin River Delta, we generally find a strong correspondence between TROPOMI SIF and the three wetland sites (r^2 = 0.42, ~~0.48, and 0.29~~ 0.42, and 0.30 for US-Tw1, US-Tw4, and US-Tw5). The inter-site differences in GPP within a single ecosystem are larger than the SIF-GPP differences, indicating some fine-scale heterogeneity that is likely not being captured here. In any case, the reasonable agreement with the GPP at the wetland sites is encouraging because standing water can often bias reflectance-based indices, particularly in the NIR (Gamon et al., 2013).

From this SIF-GPP comparison in Fig. 5, we infer a SIF-GPP scaling factor of 18.5±4.9 [(μmol/m^2/s)/(mW/m^2/sr/nm)] across the six sites in Fig. 5 (range of scaling factors is 13-25, see Fig. S3). Our comparison of TROPOMI SIF with GPP from AmeriFlux sites in California indicates larger inter-ecosystem differences in the SIF-GPP relationship than intra-ecosystem differences, lending credence to this universal scaling factor. However, there are two important caveats: 1) we do not have an eddy covariance site in an evergreen forest, which is a major limitation as much of California is dominated by evergreen forests and 2) we are not directly measuring GPP with SIF. As such, we refer to this SIF-estimated GPP as:

$$\mathrm{GPP}^* := 18.5 \cdot \mathrm{SIF}. \tag{9}$$

This single scaling from Eq. 9 seems to be a reasonable relation given the available information, with the caveat that there could be differences between ecosystems that are unaccounted for. To reiterate, there is an clear correspondence between the observed SIF and GPP estimated for the different AmeriFlux sites (see Fig. 5) but we have a limited number of AmeriFlux sites in California that do not cover all ecosystems. As such, we do not report GPP here and have included an asterisk to highlight the caveats with the relationship presented here. Future work to obtain a more robust SIF-GPP relationship covering more ecosystems is warranted.

5 Timing and spatial patterns of photosynthesis in California

Figure 6a shows the SIF-derived seasonal cycle of photosynthesis in California. One of the most prominent features is the apparent double peak in the seasonal cycle. This double peak is present in both 2018 and 2019 with similar timing of the

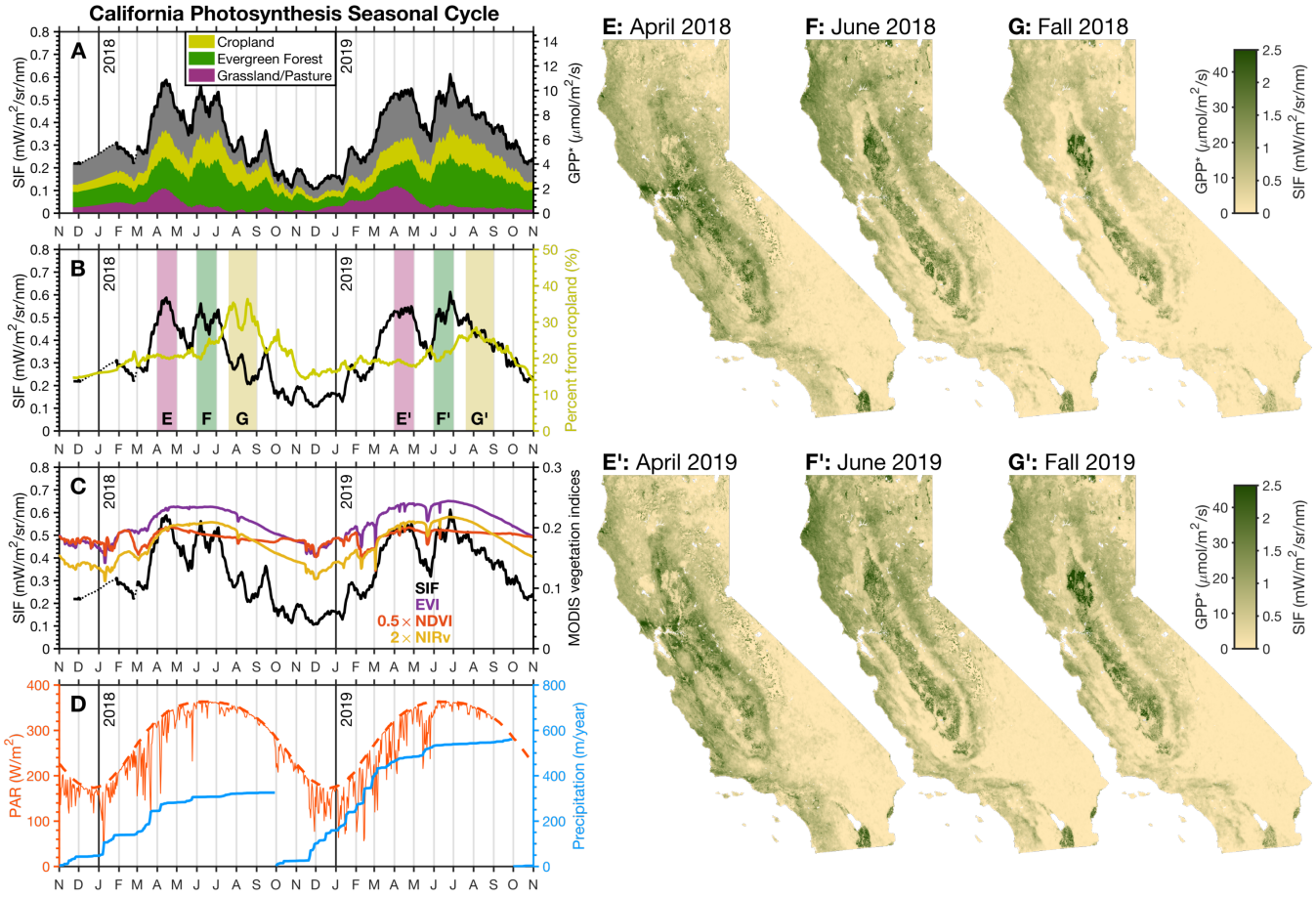

Figure 6. Seasonal cycle of photosynthesis in California. Panel A shows the statewide mean SIF (black line) at 13:30 PST from November 2017 through ~~September~~ November 2019 broken down by the contributions coming from cropland (yellow), evergreen forests (green), grasslands or pastures (purple), and other (gray). Rice is included in cropland here. Land types are taken from the 2018 CropScape database shown in Figure 1. Right axis shows the estimated GPP* based on comparison with AmeriFlux sites in California. **Panel B** shows the percentage of SIF coming from cropland (yellow). Vertical bars indicate the time periods with corresponding spatial plots in Panels E–G'. **Panel C** shows the vegetation indices (NDVI, EVI, and NIR_V) from MODIS over the same time period. **Panel D** shows clear sky PAR over California at 13:00 PST (dashed red line), surface PAR estimated from the ERA-Interim Reanalysis (thin red line), and cumulative precipitation over the water year from the GPM satellite (blue). **Panels E–G'** show the spatial patterns of SIF for the time periods indicated in Panel B.

maxima. The first peak occurs in April and the second peak occurs in June. Interestingly, the trough between the these peaks occurs near the annual maximum in PAR (red line in Fig. 6d). This begs the question: *"What is driving this double peak in the seasonality of California's photosynthesis?"*

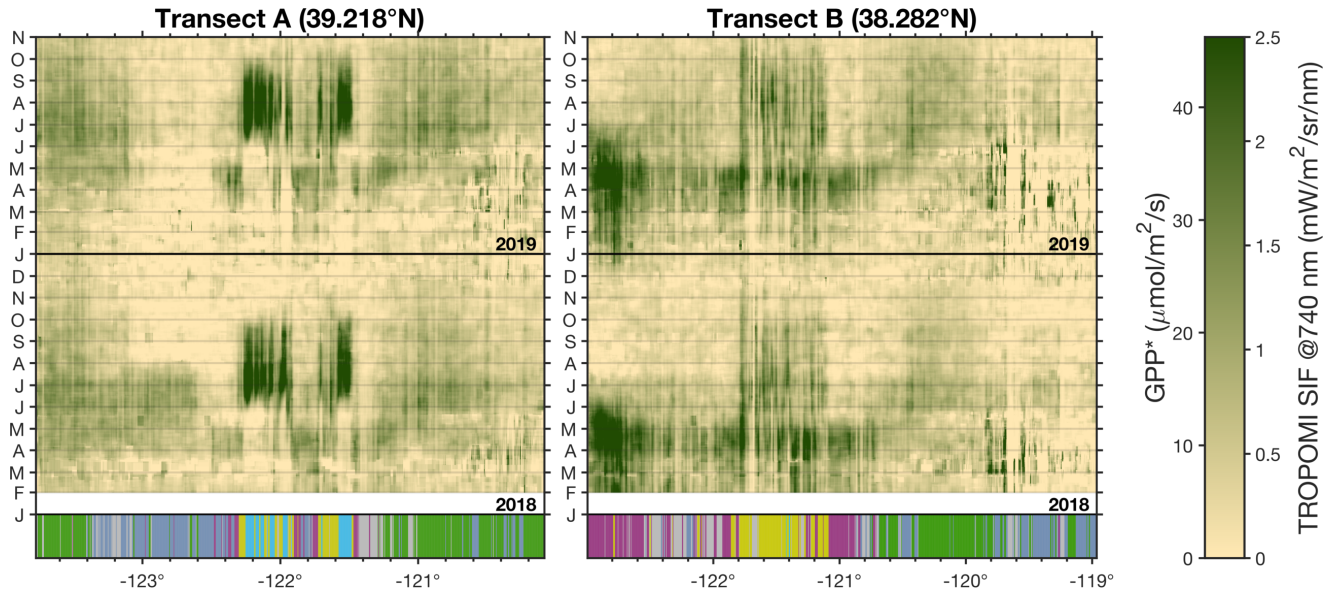

Figure 7. Hovmöller diagrams for three transects across California. Panels show Hovmöller diagrams from ~~November 2017~~ February 2018 through ~~March~~ November 2019 for the two transects shown in Fig. 1. Bottom bar indicates the dominant land type with coloring from Fig. 1: green is evergreen forest, purple is grassland/pasture, cyan is rice, yellow is cropland (excluding rice), blue is shrubland, and gray is other.

We can use the CropScape database (see Fig. 1) to determine the ecosystems driving the spatio-temporal patterns in the TROPOMI SIF data as it provides land cover classifications across the state of California at 30-m spatial resolution. However, a notable limitation of the classifications from the CropScape data is the lack of discrimination for non-cropland areas. For example, grasslands and pastures are combined into a single land type that seems to also include regions that would typically be defined as oak savanna and chaparral. In lieu of a better sub-kilometer land cover dataset, we use the classifications from the CropScape database for this work.

Figure 6a shows a breakdown of the regions contributing to the statewide SIF signal based on the land cover data from the CropScape database. We find the California grasslands and pastures (a single classification that also includes chaparral and oak savanna) have a single peak that coincides with the first statewide peak in April, this is consistent with the seasonal cycle at California grassland sites in the AmeriFlux network (Fig. 5) that show a unimodal peak in the spring that ends in May. Figs. 6e and 6e' show the mean spatial pattern in April 2018 and 2019, respectively, where we see that the April peak coincides with a statewide increase in SIF. There are a few pertinent hotspots in grasslands or pastures during this April peak. Notably, California's Central Valley and surrounding hills exhibit a strong photosynthesis signal in April. The valley to the east

of Bodega Bay (38.3°N, 122.9°W) appears as a large hotspot in both 2018 and 2019. This region lies on Transect B in Fig. 1 and the seasonal cycle is shown in more detail in Fig. 7.

The second peak in June shows a dominant contribution from evergreen forests (Fig. 6a). This can also be seen in the spatial patterns from Fig. 6f and 6f' where the evergreen forests in Northern California exhibit a strong SIF signal. California's Central Valley can be clearly distinguished as the surrounding hills have dried out (predominantly oak savanna and chaparral). The observed photosynthesis from the Central Valley is maintained by heavily irrigated cropland throughout the valley.

The yellow line in Fig. 6b indicates the fraction of SIF in California that comes from cropland. We see the largest relative contribution occurring in the fall. However, this is is primarily because all other ecosystems have gone dormant (see Fig. 6g) as opposed to an increase in photosynthetic activity from cropland. The only region that shows an increase in photosynthesis are the rice fields in the Sacramento Valley (the valley surrounding Sutter Buttes at 39.1°N, 121.5°W) in Northern California. The rice fields show a SIF signal in excess of 2.5 mW/m^2/sr/nm during the fall (GPP* in excess of 45 μmol/m^2/s).

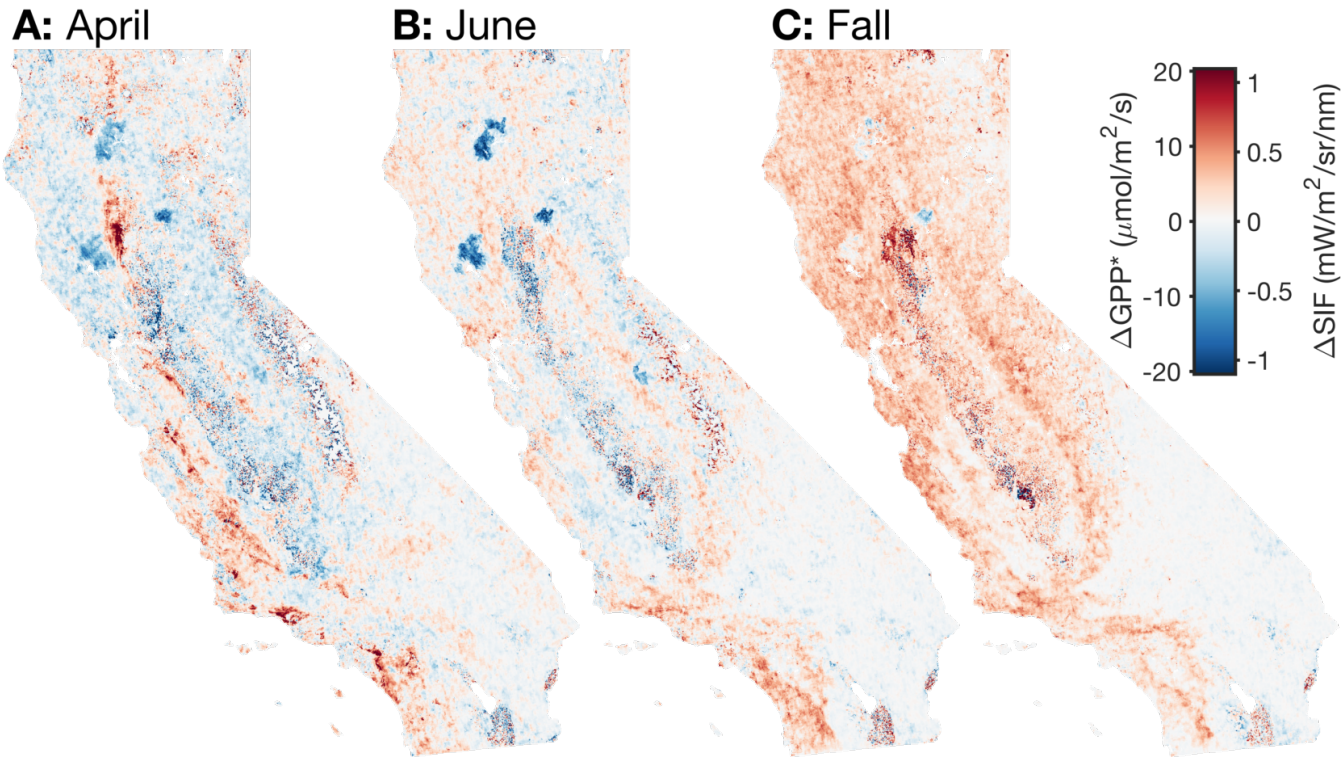

Figure 8. Difference between 2019 and 2018. Panel A shows the difference between the mean SIF in April 2019 and 2018. **Panel B** and **Panel C** are the same as ~~panel A~~ **Panel A** but for June and Fall (July 20-August 31), respectively. Red indicates higher SIF in 2019, blue indicates higher SIF in 2018.

Both 2018 and 2019 show a double peak in the seasonal cycle, however, the onset of the grassland driven peak differs substantially between the two years. This difference is likely driven by the increased precipitation in 2019 (blue line in Fig. 6d).

There was 50% more precipitation in 2019 compared to 2018 and the precipitation occurred earlier in the water year. By mid-February 2019 there was more precipitation than the annual total from 2018. This early precipitation allowed for an earlier and longer growing season for the grasses. Figure 8 shows the difference in spatial patterns between 2019 and 2018. In general, we find reasonable consistency between the two years ~~.~~ in April and June but substantial differences in the Fall. We find a factor of 2 increase in statewide SIF between fall 2018 and 2019. This increase from 2018 to 2019 is exhibited across all ecosystems. This is, again, likely due to the increased precipitation in 2019 compared to 2018. The MODIS vegetation indices show negligible differences between fall 2019 and 2018 (see Supplemental Figures S6 and S7). Most of the major differences in April and June are due to ecosystem disturbances such as fires. The 2018 Northern California fires are a striking example of that (three large negative anomalies in Fig. 8b), the impact of these fires is currently the focus of forthcoming work. An additional feature that stands out is the positive SIF anomaly in Southern California, this increase in 2019 is due to the low rainfall the previous year.

Interestingly, none of the MODIS vegetation indices (NDVI, EVI, or NIR_v) show this double peak in photosynthesis (Fig. 6c). The seasonal cycles from the three vegetation indices show a greening that starts in mid-winter (begins in December 2018) and increases roughly linearly to a peak in April. All three vegetation indices maintain that peak until July when they show a roughly linear decline through the Fall. The seasonal cycle of the three MODIS vegetation indices bear a strong similarity to the clear sky PAR seasonal cycle. This difference between SIF and the MODIS vegetation indices may be due to a clear sky bias as the reflectance-based vegetation indices (NDVI, EVI, and NIR_v) can only be made under clear sky conditions, whereas SIF can be retrieved in the presence of some clouds and aerosols (Frankenberg et al., 2011b). This is inferred by the decline in PAR during May 2018 and May 2019 (Fig. 6d) that corresponds with a decline in SIF. This highlights one of the differences between SIF and the MODIS vegetation indices, the vegetation indices are reflectance-based products whereas SIF is a fluorescence signal emitted during photosynthesis and is thus coupled to the radiation regime. This again gets back to the idea that SIF is measuring photosynthetic activity whereas the MODIS indices are measuring photosynthetic capacity.

Several ecophysiological reasons could also explain the SIF detection of a double peak feature, whereas MODIS vegetation indices do not. Nearly 11% of the state of California consists of the California oak savanna (many in the foothills of coastal mountains and the Sierras; Tyler et al., 2006). Over the course of the season, these ecosystems operate as an evergreen ecosystem, whereby understory grass is photosynthetically active during the winter months, while trees (primarily oak species) reach extremely high values of maximum carboxylation capacity (V_{cmax}) during the spring when water is plentiful, and then retain their leaves throughout the summer in a highly photoprotective state (i.e., US-Ton; Xu and Baldocchi, 2003). Spatially, we observe increased SIF values in oak savanna as well as chaparral ecosystems (also present on coastal and Sierra foothills) in the early spring when available soil moisture is at a maximum (Xu and Baldocchi, 2004; Xu et al., 2004). As these ecosystems enter the hot, dry summers, increases in sustained non-photochemical quenching and decreases in photochemistry result in decreased fluorescence, while still appearing "green" to MODIS vegetation indices. Meanwhile, snow is melting rapidly at higher elevations, making water available for many of the needleleaf evergreen species in the Sierras and Coastal ranges, then the water resources become depleted and temperatures cool prompting these evergreen species to go back into a photoprotective state, resulting in a short photosynthetically active growing season that has been shown to be more well characterized by

SIF from GOME-2 than MODIS NDVI and EVI (Zuromski et al., 2018). Future work comparing SIF and MODIS indices with measured PAR at AmeriFlux sites would be useful in further evaluating the role of radiation and physiology in the double peak feature.

Figure 7 shows a Hovmöller diagram for three transects across Northern California (see Figure 1 for the location of the transects). Transect A in Figure 7 shows the short but strong SIF signal from the rice fields. The timing of the SIF signal from the rice fields agrees with the growing cycle for rice in California. Rice in the Sacramento Valley is typically planted in mid-to-late May, the fields are then flooded, and harvested in mid-to-late September (University of California at Davis, 2018). This observation of the rice fields is encouraging because we are observing photosynthesis in the presence of standing water, which can often bias reflectance-based indices in the NIR (Gamon et al., 2013). In both 2018 and 2019 we observe the onset of photosynthesis at the rice fields in the first few days of June and a rapid decline at the end of September. Transect B begins in the valley to the east of Bodega Bay (location of the grassland hotspot) and crosses the central valley. This grassland hotspot is present from April through May of both 2018 and 2019. The valley near Bodega Bay is dominated by pastures, however it is currently unclear why this particular region exhibits a stronger SIF signal than other pastures in California. The persistent strong signal in 2018 and 2019 might make it an interesting site for study with an eddy covariance site in the future.

6 Dominant "modes" of variability in California's photosynthesis

Section 5 discussed the spatio-temporal patterns for different regions and ecosystems, here we present an alternative method of characterizing the dominant modes of spatio-temporal variability in photosynthesis using Empirical Orthogonal Functions (EOFs) and their associated Principal Components (PCs). EOFs are a matrix factorization that are commonly used to identify structure in a spatial dataset and yield a finite number of modes. These modes compactly represent the data and are often interpreted as physical modes of the system.

Figure 9 shows the first two EOFs and their associated PCs for the TROPOMI SIF data over California, the corresponding eigenvalue spectrum can be seen in Fig. S5. The first two EOFs corroborate the findings from Section 5 and, taken together, explain 84% of the variability in the TROPOMI SIF data:

- EOF 1: the mean signal
- EOF 2: the double peak

The first EOF (Fig. 9a) represents the mean signal and explains ~~73~~74% of the variability in the TROPOMI SIF data. From the spatial pattern we can see that it includes most of the biomass in California and is strongly correlated to the state-wide mean SIF: r^2 = 0.99. The associated principal component bears a strong similarity to the statewide mean SIF seasonal cycle (Fig. 6a). This finding is not entirely surprising because we are using un-normalized SIF data for the matrix factorization. This means that the most important mode of variability is the mean signal and that the following EOFs are anomalies relative to the mean signal.

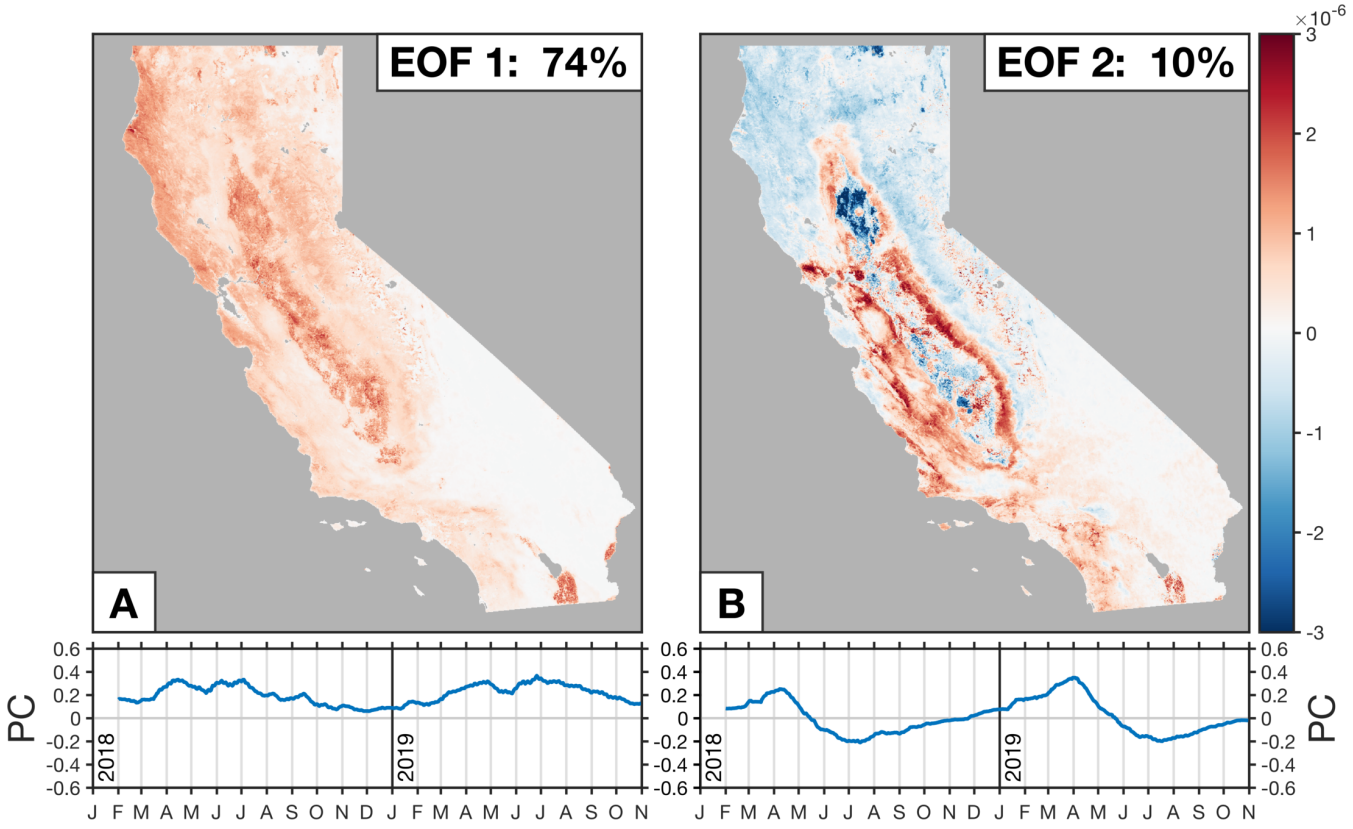

Figure 9. EOFs and PCs for TROPOMI SIF over California. Panels show the first two EOFs and PCs. EOFs are unit length (sum of the squares is equal to 1) and computed using unnormalized SIF spatially downscaled with NIR_V. Time series show the corresponding PC (blue line) from February 2018 through ~~September~~ November 2019. Length of the PC is equal to the corresponding eigenvalue and has units of mW/m^2/sr/nm. Text in figure lists the percent of variance explained by that EOF. Fig. S5 shows the corresponding eigenvalue spectrum for the TROPOMI SIF data over California.

The second EOF (Fig. 9b) represents the double peak in the timing of California's photosynthesis. This EOF combines the signal from the grasslands (positive phase of EOF 2) and the evergreen forests (negative phase of EOF 2). We find EOF 2 to be positively correlated with the grassland fraction from the CropScape database (r = 0.55) and negatively correlated with the evergreen forests (r = ~~-0.37~~-0.36). There is also a negative correlation with the rice fields (r = ~~-0.31~~-0.32). The associated principle component serves to amplify the seasonal cycle from EOF 1 in grasslands during April and amplify the forest peak in June. This is because the red region (grasslands) in Fig. 9b will contribute a positive anomaly in April and a negative anomaly in June. Conversely, the blue region (evergreen forests and rice) will contribute a negative anomaly in April and a positive anomaly in June. This EOF arises because the grasslands and forests are both spatially separated and out of phase with each other, allowing the matrix factorization to place them into a single EOF that represents the processes driving the double peak in the timing of California's photosynthesis.

It should be noted that these EOF patterns found here are unlikely to be true "physical modes" (see, for example, Monahan et al., 2009). That is to say, we would not necessarily expect the response to a perturbation to follow patterns shown in Fig. 9. EOF 2 is a good example of this because it seems unlikely that the grasslands and forests will exhibit opposing responses to a forcing. Grasslands and forests are combined into a single EOF simply because there is little loss of information by combining them due to the spatial separation and phase offset. This is not to argue against the utility of EOFs. EOFs are a useful method for identifying structure in geophysical datasets, as evidenced here by their identification of the double peak in the timing of California's photosynthesis.

7 Conclusions

We present an oversampling and downscaling method to ~~obtain~~ produce daily estimates of Solar Induced chlorophyll Fluorescence (SIF), a proxy for photosynthetic activity, at 500-m spatial resolution from TROPOMI. To our knowledge, this is the highest spatial resolution SIF dataset from satellite measurements. We find a double peak in the seasonality of photosynthesis in California during 2018 and 2019, a feature that is not present in the MODIS vegetation indices (NDVI, EVI, or NIR_V). Analysis of the spatial and temporal patterns of the SIF data indicates that the double peak is due to two processes that are out of phase with each other: woody grasslands (e.g., grasslands, chaparral, and oak savanna) and evergreen forests.

Our work applies methods developed for previous satellite retrievals (oversampling) and uses estimates of sub-grid scale vegetation (downscaling) to ~~obtain~~ produce daily 500-m spatial resolution SIF from TROPOMI over California. We use a 14-day moving window to produce this esimate. The oversampling method results in a smooth spatial field and removes artifacts due to complex topography and the wide TROPOMI swath. The downscaling method further refines the high resolution spatial patterns by bringing in *a priori* information on the sub-grid vegetation patterns. The oversampling and downscaling methods do not alter the large scale spatio-temporal patterns as they conserve the SIF signal over a single scene.

TROPOMI SIF data and MODIS vegetation indices are reasonably consistent at annual timescales over California, but show weaker relationships at daily and monthly timescales. This implies that TROPOMI SIF is providing some information that is distinct from the MODIS vegetation indices. TROPOMI SIF data show a strong correspondence with half-hourly estimates of GPP at multiple AmeriFlux sites across different ecosystems including: cropland, grassland, savanna, and wetlands. We find a linear relationship between SIF and GPP that is largely invariant across ecosystems with an intercept that is not significantly different from zero. As such, we use SIF as an estimate of GPP^* with the caveat that some ecosystems are not represented in our California analysis.

~~TROPOMI SIF data show a double peak in the seasonality of photosynthesis in California, a feature that is not present in the MODIS vegetation indices.~~ The double peak in the seasonality of California's photosynthesis observed by TROPOMI SIF is due to two processes that are out of phase with each other: grasses show a maximum in April and evergreen forests peak in June. An empirical orthogonal function (EOF) analysis corroborates the phase offset and spatial patterns driving the double peak. The EOF analysis also indicates that two spatio-temporal patterns explain 84% of the variability in the TROPOMI SIF data.

The results shown here are promising for obtaining global near-daily GPP at sub-kilometer spatial scales using satellite measurements. This, in turn, may prove helpful in addressing long-standing questions regarding the mechanisms and locations driving carbon uptake in the Northern Hemisphere. It would also allow us to monitor climate change impacts on vulnerable ecosystems at local-to-global scales.

Acknowledgements. A. J. Turner is supported as a Miller Fellow with the Miller Institute for Basic Research in Science at UC Berkeley. R. C. Cohen acknowledges support from the TEMPO project SV3-83019. P. Köhler and C. Frankenberg are funded by the Earth Science U.S. participating investigator (grant: NNX15AH95G). This research used the Savio computational cluster resource provided by the Berkeley Research Computing program at the University of California, Berkeley (supported by the UC Berkeley Chancellor, Vice Chancellor for Research, and Chief Information Officer). This research also used resources from the National Energy Research Scientific Computing Center, which is supported by the Office of Science of the U.S. Department of Energy under Contract No. DE-AC02-05CH11231. TROPOMI SIF and MODIS NBAR data are publicly available at "ftp://fluo.gps.caltech.edu/data/tropomi/" and "https://e4ftl01.cr.usgs.gov/MOTA/MCD43A4.006/", respectively. Funding for AmeriFlux data resources was provided by the U.S. Department of Energy's Office of Science. We would like to thank Dennis Baldocchi (UC Berkeley) for sharing the AmeriFlux data and for providing extensive feedback on the work. Finally, we are extremely grateful to the team that has realized the TROPOMI instrument, consisting of the partnership between Airbus Defence and Space, KNMI, SRON, and TNO, commissioned by NSO and ESA.

References

Anav, A., Friedlingstein, P., Beer, C., Ciais, P., Harper, A., Jones, C., Murray-Tortarolo, G., Papale, D., Parazoo, N. C., Peylin, P., Piao, S., Sitch, S., Viovy, N., Wiltshire, A., and Zhao, M.: Spatiotemporal patterns of terrestrial gross primary production: A review, Rev Geophys, 53, 785–818, https://doi.org/10.1002/2015rg000483, 2015.

Badgley, G., Field, C. B., and Berry, J. A.: Canopy near-infrared reflectance and terrestrial photosynthesis, Sci Adv, 3, e1602 244, https://doi.org/10.1126/sciadv.1602244, 2017.

Badgley, G., Anderegg, L. D. L., Berry, J. A., and Field, C. B.: Terrestrial Gross Primary Production: Using NIR_V to Scale from Site to Globe, Global change biology, https://doi.org/10.1111/gcb.14729, 2019.

Baker, N. R.: Chlorophyll fluorescence: a probe of photosynthesis in vivo, Annual review of plant biology, 59, 89–113, https://doi.org/10.1146/annurev.arplant.59.032607.092759, 2008.

Baldocchi, D., Falge, E., Gu, L., Olson, R., Hollinger, D., Running, S., Anthoni, P., Bernhofer, C., Davis, K., Evans, R., Fuentes, J., Goldstein, A., Katul, G., Law, B., Lee, X., Malhi, Y., Meyers, T., Munger, W., Oechel, W., Paw, K. T., Pilegaard, K., Schmid, H. P., Valentini, R., Verma, S., Vesala, T., Wilson, K., and Wofsy, S.: FLUXNET: A New Tool to Study the Temporal and Spatial Variability of Ecosystem–Scale Carbon Dioxide, Water Vapor, and Energy Flux Densities, Bulletin of the American Meteorological Society, 82, 2415–2434, https://doi.org/10.1175/1520-0477(2001)082<2415:fantts>2.3.co;2, 2001.

Baldocchi, D. D., Hicks, B. B., and Meyers, T. P.: Measuring Biosphere-Atmosphere Exchanges of Biologically Related Gases with Micrometeorological Methods, Ecology, 69, 1331–1340, https://doi.org/10.2307/1941631, 1988.

Ballantyne, A. P., Alden, C. B., Miller, J. B., Tans, P. P., and White, J. W.: Increase in observed net carbon dioxide uptake by land and oceans during the past 50 years, Nature, 488, 70–2, https://doi.org/10.1038/nature11299, 2012.

Ciais, P., Tan, J., Wang, X., Roedenbeck, C., Chevallier, F., Piao, S. L., Moriarty, R., Broquet, G., Le Quere, C., Canadell, J. G., Peng, S., Poulter, B., Liu, Z., and Tans, P.: Five decades of northern land carbon uptake revealed by the interhemispheric CO_2 gradient, Nature, 568, 221–225, https://doi.org/10.1038/s41586-019-1078-6, 2019.

Drusch, M., Moreno, J., Del Bello, U., Franco, R., Goulas, Y., Huth, A., Kraft, S., Middleton, E. M., Miglietta, F., Mohammed, G., Nedbal, L., Rascher, U., Schuttemeyer, D., and Verhoef, W.: The FLuorescence EXplorer Mission Concept–ESA's Earth Explorer 8, IEEE Transactions on Geoscience and Remote Sensing, 55, 1273–1284, https://doi.org/10.1109/tgrs.2016.2621820, 2017.

Frankenberg, C., Butz, A., and Toon, G. C.: Disentangling chlorophyll fluorescence from atmospheric scattering effects in O_2A-band spectra of reflected sun-light, Geophysical Research Letters, 38, https://doi.org/10.1029/2010gl045896, 2011a.

Frankenberg, C., Fisher, J. B., Worden, J., Badgley, G., Saatchi, S. S., Lee, J.-E., Toon, G. C., Butz, A., Jung, M., Kuze, A., and Yokota, T.: New global observations of the terrestrial carbon cycle from GOSAT: Patterns of plant fluorescence with gross primary productivity, Geophys Res Lett, 38, https://doi.org/10.1029/2011gl048738, 2011b.

Frankenberg, C., O'Dell, C., Guanter, L., and McDuffie, J.: Remote sensing of near-infrared chlorophyll fluorescence from space in scattering atmospheres: implications for its retrieval and interferences with atmospheric CO_2 retrievals, Atmospheric Measurement Techniques, 5, 2081–2094, https://doi.org/10.5194/amt-5-2081-2012, 2012.

Frankenberg, C., O'Dell, C., Berry, J., Guanter, L., Joiner, J., Köhler, P., Pollock, R., and Taylor, T. E.: Prospects for chlorophyll fluorescence remote sensing from the Orbiting Carbon Observatory-2, Remote Sensing of Environment, 147, 1–12, https://doi.org/10.1016/j.rse.2014.02.007, 2014.

Gamon, J. A., Huemmrich, K. F., Stone, R. S., and Tweedie, C. E.: Spatial and temporal variation in primary productivity (NDVI) of coastal Alaskan tundra: Decreased vegetation growth following earlier snowmelt, Remote Sensing of Environment, 129, 144–153, https://doi.org/10.1016/j.rse.2012.10.030, 2013.

Guanter, L., Frankenberg, C., Dudhia, A., Lewis, P. E., Gomez-Dans, J., Kuze, A., Suto, H., and Grainger, R. G.: Retrieval and global assessment of terrestrial chlorophyll fluorescence from GOSAT space measurements, Remote Sensing of Environment, 121, 236–251, https://doi.org/10.1016/j.rse.2012.02.006, 2012.

Guanter, L., Zhang, Y., Jung, M., Joiner, J., Voigt, M., Berry, J. A., Frankenberg, C., Huete, A. R., Zarco-Tejada, P., Lee, J. E., Moran, M. S., Ponce-Campos, G., Beer, C., Camps-Valls, G., Buchmann, N., Gianelle, D., Klumpp, K., Cescatti, A., Baker, J. M., and Griffis, T. J.: Global and time-resolved monitoring of crop photosynthesis with chlorophyll fluorescence, Proceedings of the National Academy of Sciences of the United States of America, 111, E1327–33, https://doi.org/10.1073/pnas.1320008111, 2014.

Guanter, L., Aben, I., Tol, P., Krijger, J. M., Hollstein, A., Köhler, P., Damm, A., Joiner, J., Frankenberg, C., and Landgraf, J.: Potential of the TROPOspheric Monitoring Instrument (TROPOMI) onboard the Sentinel-5 Precursor for the monitoring of terrestrial chlorophyll fluorescence, Atmospheric Measurement Techniques, 8, 1337–1352, https://doi.org/10.5194/amt-8-1337-2015, 2015.

Hemes, K. S., Chamberlain, S. D., Eichelmann, E., Anthony, T., Valach, A., Kasak, K., Szutu, D., Verfaillie, J., Silver, W. L., and Baldocchi, D. D.: Assessing the carbon and climate benefit of restoring degraded agricultural peat soils to managed wetlands, Agricultural and Forest Meteorology, 268, 202–214, https://doi.org/10.1016/j.agrformet.2019.01.017, 2019.

IPCC: Climate Change 2013: The Physical Science Basis. Contribution of Working Group I to the Fifth Assessment Report of the Intergovernmental Panel on Climate Change, Tech. rep., IPCC, 2013.

Jeong, S.-J., Schimel, D., Frankenberg, C., Drewry, D. T., Fisher, J. B., Verma, M., Berry, J. A., Lee, J.-E., and Joiner, J.: Application of satellite solar-induced chlorophyll fluorescence to understanding large-scale variations in vegetation phenology and function over northern high latitude forests, Remote Sensing of Environment, 190, 178–187, https://doi.org/10.1016/j.rse.2016.11.021, 2017.

Joiner, J., Yoshida, Y., Vasilkov, A. P., Yoshida, Y., Corp, L. A., and Middleton, E. M.: First observations of global and seasonal terrestrial chlorophyll fluorescence from space, Biogeosciences, 8, 637–651, https://doi.org/10.5194/bg-8-637-2011, 2011.

Joiner, J., Yoshida, Y., Vasilkov, A. P., Middleton, E. M., Campbell, P. K. E., Yoshida, Y., Kuze, A., and Corp, L. A.: Filling-in of near-infrared solar lines by terrestrial fluorescence and other geophysical effects: simulations and space-based observations from SCIAMACHY and GOSAT, Atmospheric Measurement Techniques, 5, 809–829, https://doi.org/10.5194/amt-5-809-2012, 2012.

Joiner, J., Guanter, L., Lindstrot, R., Voigt, M., Vasilkov, A. P., Middleton, E. M., Huemmrich, K. F., Yoshida, Y., and Frankenberg, C.: Global monitoring of terrestrial chlorophyll fluorescence from moderate-spectral-resolution near-infrared satellite measurements: methodology, simulations, and application to GOME-2, Atmospheric Measurement Techniques, 6, 2803–2823, https://doi.org/10.5194/amt-6-2803-2013, 2013.

Joiner, J., Yoshida, Y., Vasilkov, A. P., Schaefer, K., Jung, M., Guanter, L., Zhang, Y., Garrity, S., Middleton, E. M., Huemmrich, K. F., Gu, L., and Belelli Marchesini, L.: The seasonal cycle of satellite chlorophyll fluorescence observations and its relationship to vegetation phenology and ecosystem atmosphere carbon exchange, Remote Sensing of Environment, 152, 375–391, https://doi.org/10.1016/j.rse.2014.06.022, 2014.

Joiner, J., Yoshida, Y., Guanter, L., and Middleton, E. M.: New methods for the retrieval of chlorophyll red fluorescence from hyperspectral satellite instruments: simulations and application to GOME-2 and SCIAMACHY, Atmospheric Measurement Techniques, 9, 3939–3967, https://doi.org/10.5194/amt-9-3939-2016, 2016.

Köhler, P., Guanter, L., and Joiner, J.: A linear method for the retrieval of sun-induced chlorophyll fluorescence from GOME-2 and SCIAMACHY data, Atmospheric Measurement Techniques, 8, 2589–2608, https://doi.org/10.5194/amt-8-2589-2015, 2015.

Köhler, P., Frankenberg, C., Magney, T. S., Guanter, L., Joiner, J., and Landgraf, J.: Global Retrievals of Solar-Induced Chlorophyll Fluorescence With TROPOMI: First Results and Intersensor Comparison to OCO-2, Geophysical Research Letters, 45, 10,456–10,463, https://doi.org/10.1029/2018gl079031, 2018.

Kuze, A., Suto, H., Nakajima, M., and Hamazaki, T.: Thermal and near infrared sensor for carbon observation Fourier-transform spectrometer on the Greenhouse Gases Observing Satellite for greenhouse gases monitoring, Appl Opt, 48, 6716–33, https://doi.org/10.1364/AO.48.006716, 2009.

Lee, J. E., Frankenberg, C., van der Tol, C., Berry, J. A., Guanter, L., Boyce, C. K., Fisher, J. B., Morrow, E., Worden, J. R., Asefi, S., Badgley, G., and Saatchi, S.: Forest productivity and water stress in Amazonia: observations from GOSAT chlorophyll fluorescence, Proc. Biol. Sci., 280, 20130 171, https://doi.org/10.1098/rspb.2013.0171, 2013.

Li, X. and Xiao, J.: A Global, 0.05-Degree Product of Solar-Induced Chlorophyll Fluorescence Derived from OCO-2, MODIS, and Reanalysis Data, Remote Sensing, 11, 517, https://doi.org/10.3390/rs11050517, 2019.

Liu, L., Guan, L., and Liu, X.: Directly estimating diurnal changes in GPP for C3 and C4 crops using far-red sun-induced chlorophyll fluorescence, Agricultural and Forest Meteorology, 232, 1–9, https://doi.org/10.1016/j.agrformet.2016.06.014, 2017.

Luus, K. A., Commane, R., Parazoo, N. C., Benmergui, J., Euskirchen, E. S., Frankenberg, C., Joiner, J., Lindaas, J., Miller, C. E., Oechel, W. C., Zona, D., Wofsy, S., and Lin, J. C.: Tundra photosynthesis captured by satellite-observed solar-induced chlorophyll fluorescence, Geophysical Research Letters, 44, 1564–1573, https://doi.org/10.1002/2016gl070842, 2017.

Magney, T. S., Frankenberg, C., Fisher, J. B., Sun, Y., North, G. B., Davis, T. S., Kornfeld, A., and Siebke, K.: Connecting active to passive fluorescence with photosynthesis: a method for evaluating remote sensing measurements of Chl fluorescence, The New phytologist, 215, 1594–1608, https://doi.org/10.1111/nph.14662, 2017.

Magney, T. S., Bowling, D. R., Logan, B. A., Grossmann, K., Stutz, J., Blanken, P. D., Burns, S. P., Cheng, R., Garcia, M. A., Köhler, P., Lopez, S., Parazoo, N. C., Raczka, B., Schimel, D., and Frankenberg, C.: Mechanistic evidence for tracking the seasonality of photosynthesis with solar-induced fluorescence, Proceedings of the National Academy of Sciences of the United States of America, 116, 11 640–11 645, https://doi.org/10.1073/pnas.1900278116, 2019a.

Magney, T. S., Frankenberg, C., Köhler, P., North, G., Davis, T. S., Dold, C., Dutta, D., Fisher, J. B., Grossmann, K., Harrington, A., Hatfield, J., Stutz, J., Sun, Y., and Porcar-Castell, A.: Disentangling changes in the spectral shape of chlorophyll fluorescence: Implications for remote sensing of photosynthesis, Journal of Geophysical Research: Biogeosciences, https://doi.org/10.1029/2019jg005029, 2019b.

Mahadevan, P., Wofsy, S. C., Matross, D. M., Xiao, X., Dunn, A. L., Lin, J. C., Gerbig, C., Munger, J. W., Chow, V. Y., and Gottlieb, E. W.: A satellite-based biosphere parameterization for net ecosystem CO_2 exchange: Vegetation Photosynthesis and Respiration Model (VPRM), Global Biogeochemical Cycles, 22, https://doi.org/10.1029/2006gb002735, 2008.

Mohammed, G. H., Colombo, R., Middleton, E. M., Rascher, U., van der Tol, C., Nedbal, L., Goulas, Y., Perez-Priego, O., Damm, A., Meroni, M., Joiner, J., Cogliati, S., Verhoef, W., Malenovsky, Z., Gastellu-Etchegorry, J.-P., Miller, J. R., Guanter, L., Moreno, J., Moya, I., Berry, J. A., Frankenberg, C., and Zarco-Tejada, P. J.: Remote sensing of solar-induced chlorophyll fluorescence (SIF) in vegetation: 50 years of progress, Remote Sensing of Environment, 231, 111 177, https://doi.org/10.1016/j.rse.2019.04.030, 2019.

Monahan, A. H., Fyfe, J. C., Ambaum, M. H. P., Stephenson, D. B., and North, G. R.: Empirical Orthogonal Functions: The Medium is the Message, Journal of Climate, 22, 6501–6514, https://doi.org/10.1175/2009jcli3062.1, 2009.

Monteith, J. L.: Solar Radiation and Productivity in Tropical Ecosystems, Journal of Applied Ecology, 9, 747–766, 1972.

Parazoo, N. C., Bowman, K., Fisher, J. B., Frankenberg, C., Jones, D. B., Cescatti, A., Perez-Priego, O., Wohlfahrt, G., and Montagnani, L.: Terrestrial gross primary production inferred from satellite fluorescence and vegetation models, Global change biology, 20, 3103–21, https://doi.org/10.1111/gcb.12652, 2014.

Parazoo, N. C., Arneth, A., Pugh, T. A. M., Smith, B., Steiner, N., Luus, K., Commane, R., Benmergui, J., Stofferahn, E., Liu, J., Rodenbeck, C., Kawa, R., Euskirchen, E., Zona, D., Arndt, K., Oechel, W., and Miller, C.: Spring photosynthetic onset and net CO_2 uptake in Alaska triggered by landscape thawing, Global change biology, 24, 3416–3435, https://doi.org/10.1111/gcb.14283, 2018.

Parazoo, N. C., Frankenberg, C., Kohler, P., Joiner, J., Yoshida, Y., Magney, T., Sun, Y., and Yadav, V.: Towards a Harmonized Long-Term Spaceborne Record of Far-Red Solar-Induced Fluorescence, Journal of Geophysical Research: Biogeosciences, https://doi.org/10.1029/2019jg005289, 2019.

Peters, W., Jacobson, A. R., Sweeney, C., Andrews, A. E., Conway, T. J., Masarie, K., Miller, J. B., Bruhwiler, L. M., Petron, G., Hirsch, A. I., Worthy, D. E., van der Werf, G. R., Randerson, J. T., Wennberg, P. O., Krol, M. C., and Tans, P. P.: An atmospheric perspective on North American carbon dioxide exchange: CarbonTracker, Proc Natl Acad Sci, 104, 18 925–30, https://doi.org/10.1073/pnas.0708986104, 2007.

Reichstein, M., Falge, E., Baldocchi, D., Papale, D., Aubinet, M., Berbigier, P., Bernhofer, C., Buchmann, N., Gilmanov, T., Granier, A., Grunwald, T., Havrankova, K., Ilvesniemi, H., Janous, D., Knohl, A., Laurila, T., Lohila, A., Loustau, D., Matteucci, G., Meyers, T., Miglietta, F., Ourcival, J.-M., Pumpanen, J., Rambal, S., Rotenberg, E., Sanz, M., Tenhunen, J., Seufert, G., Vaccari, F., Vesala, T., Yakir, D., and Valentini, R.: On the separation of net ecosystem exchange into assimilation and ecosystem respiration: review and improved algorithm, Global change biology, 11, 1424–1439, https://doi.org/10.1111/j.1365-2486.2005.001002.x, 2005.

Schaaf, C. B., Gao, F., Strahler, A. H., Lucht, W., Li, X., Tsang, T., Strugnell, N. C., Zhang, X., Jin, Y., Muller, J.-P., Lewis, P., Barnsley, M., Hobson, P., Disney, M., Roberts, G., Dunderdale, M., Doll, C., d'Entremont, R. P., Hu, B., Liang, S., Privette, J. L., and Roy, D.: First operational BRDF, albedo nadir reflectance products from MODIS, Remote Sensing of Environment, 83, 135–148, https://doi.org/10.1016/s0034-4257(02)00091-3, 2002.

Sellers, P. J., Mintz, Y., Sud, Y. C., and Dalcher, A.: A Simple Biosphere Model (SIB) for Use within General Circulation Models, Journal of the Atmospheric Sciences, 43, 505–531, https://doi.org/10.1175/1520-0469(1986)043<0505:asbmfu>2.0.co;2, 1986.

Strahler, A., Muchoney, D., Borak, J., Friedl, F., Gopal, S., Lambin, L., and Moody, A.: MODIS Land Cover Product Algorithm Theoretical Basis Document (ATBD), Tech. rep., Center for Remote Sensing, Department of Geography, Boston University, https://modis.gsfc.nasa.gov/data/atbd/atbd_mod12.pdf, 1999.

Sun, K., Zhu, L., Cady-Pereira, K., Chan Miller, C., Chance, K., Clarisse, L., Coheur, P.-F., Gonzalez Abad, G., Huang, G., Liu, X., Van Damme, M., Yang, K., and Zondlo, M.: A physics-based approach to oversample multi-satellite, multispecies observations to a common grid, Atmospheric Measurement Techniques, 11, 6679–6701, https://doi.org/10.5194/amt-11-6679-2018, 2018a.

Sun, Y., Frankenberg, C., Wood, J. D., Schimel, D. S., Jung, M., Guanter, L., Drewry, D. T., Verma, M., Porcar-Castell, A., Griffis, T. J., Gu, L., Magney, T. S., Kohler, P., Evans, B., and Yuen, K.: OCO-2 advances photosynthesis observation from space via solar-induced chlorophyll fluorescence, Science, 358, https://doi.org/10.1126/science.aam5747, 2017.

Sun, Y., Frankenberg, C., Jung, M., Joiner, J., Guanter, L., Köhler, P., and Magney, T.: Overview of Solar-Induced chlorophyll Fluorescence (SIF) from the Orbiting Carbon Observatory-2: Retrieval, cross-mission comparison, and global monitoring for GPP, Remote Sensing of Environment, 209, 808–823, https://doi.org/10.1016/j.rse.2018.02.016, 2018b.

Tans, P. P., Fung, I. Y., and Takahashi, T.: Observational contrains on the global atmospheric CO_2 budget, Science, 247, 1431–8, https://doi.org/10.1126/science.247.4949.1431, 1990.

Tyler, C. M., Kuhn, B., and Davis, F. W.: Demography and recruitment limitations of three oak species in California, Q Rev Biol, 81, 127–52, 2006.

University of California at Davis: Rice Production Manual, Tech. rep., California Rice Production Workshop, Davis, CA, http://rice.ucanr.edu/files/288581.pdf, 2018.

USDA: National Agricultural Statistics Service Cropland Data Layer: Published crop-specific data layer, https://nassgeodata.gmu.edu/CropScape/, 2018.

USGCRP: Second State of the Carbon Cycle Report (SOCCR2): A Sustained Assessment Report, Tech. rep., U.S. Global Change Research Program, https://doi.org/10.7930/SOCCR2.2018, 2018.

Veefkind, J. P., Aben, I., McMullan, K., Förster, H., de Vries, J., Otter, G., Claas, J., Eskes, H. J., de Haan, J. F., Kleipool, Q., van Weele, M., Hasekamp, O., Hoogeveen, R., Landgraf, J., Snel, R., Tol, P., Ingmann, P., Voors, R., Kruizinga, B., Vink, R., Visser, H., and Levelt, P. F.: TROPOMI on the ESA Sentinel-5 Precursor: A GMES mission for global observations of the atmospheric composition for climate, air quality and ozone layer applications, Proc SPIE, 120, 70–83, https://doi.org/10.1016/j.rse.2011.09.027, 2012.

Walther, S., Voigt, M., Thum, T., Gonsamo, A., Zhang, Y., Kohler, P., Jung, M., Varlagin, A., and Guanter, L.: Satellite chlorophyll fluorescence measurements reveal large-scale decoupling of photosynthesis and greenness dynamics in boreal evergreen forests, Global change biology, 22, 2979–96, https://doi.org/10.1111/gcb.13200, 2016.

Xu, L. and Baldocchi, D. D.: Seasonal trends in photosynthetic parameters and stomatal conductance of blue oak (Quercus douglasii) under prolonged summer drought and high temperature, Tree Physiol, 23, 865–77, https://doi.org/10.1093/treephys/23.13.865, 2003.

Xu, L. and Baldocchi, D. D.: Seasonal variation in carbon dioxide exchange over a Mediterranean annual grassland in California, Agricultural and Forest Meteorology, 123, 79–96, https://doi.org/10.1016/j.agrformet.2003.10.004, 2004.

Xu, L., Baldocchi, D. D., and Tang, J.: How soil moisture, rain pulses, and growth alter the response of ecosystem respiration to temperature, Global Biogeochemical Cycles, 18, https://doi.org/10.1029/2004gb002281, 2004.

Yang, H., Yang, X., Zhang, Y., Heskel, M. A., Lu, X., Munger, J. W., Sun, S., and Tang, J.: Chlorophyll fluorescence tracks seasonal variations of photosynthesis from leaf to canopy in a temperate forest, Global change biology, 23, 2874–2886, https://doi.org/10.1111/gcb.13590, 2017.

Yang, K., Ryu, Y., Dechant, B., Berry, J. A., Hwang, Y., Jiang, C., Kang, M., Kim, J., Kimm, H., Kornfeld, A., and Yang, X.: Sun-induced chlorophyll fluorescence is more strongly related to absorbed light than to photosynthesis at half-hourly resolution in a rice paddy, Remote Sensing of Environment, 216, 658–673, https://doi.org/10.1016/j.rse.2018.07.008, 2018.

Yang, P. and van der Tol, C.: Linking canopy scattering of far-red sun-induced chlorophyll fluorescence with reflectance, Remote Sensing of Environment, 209, 456–467, https://doi.org/10.1016/j.rse.2018.02.029, 2018.

Yang, X., Tang, J., Mustard, J. F., Lee, J.-E., Rossini, M., Joiner, J., Munger, J. W., Kornfeld, A., and Richardson, A. D.: Solar-induced chlorophyll fluorescence that correlates with canopy photosynthesis on diurnal and seasonal scales in a temperate deciduous forest, Geophysical Research Letters, 42, 2977–2987, https://doi.org/10.1002/2015gl063201, 2015.

Yu, L., Wen, J., Chang, C. Y., Frankenberg, C., and Sun, Y.: High-Resolution Global Contiguous SIF of OCO-2, Geophysical Research Letters, 46, 1449–1458, https://doi.org/10.1029/2018gl081109, 2019.

Zeng, Y., Badgley, G., Dechant, B., Ryu, Y., Chen, M., and Berry, J. A.: A practical approach for estimating the escape ratio of near-infrared solar-induced chlorophyll fluorescence, Remote Sensing of Environment, 232, https://doi.org/10.1016/j.rse.2019.05.028, 2019.

Zhang, Y., Joiner, J., Alemohammad, S. H., Zhou, S., and Gentine, P.: A global spatially contiguous solar-induced fluorescence (CSIF) dataset using neural networks, Biogeosciences, 15, 5779–5800, https://doi.org/10.5194/bg-15-5779-2018, 2018.

Zhu, L., Jacob, D. J., Mickley, L. J., Marais, E. A., Cohan, D. S., Yoshida, Y., Duncan, B. N., Gonzalez Abad, G., and Chance, K. V.: Anthropogenic emissions of highly reactive volatile organic compounds in eastern Texas inferred from oversampling of satellite (OMI) measurements of HCHO columns, Environmental Research Letters, 9, 114 004, https://doi.org/10.1088/1748-9326/9/11/114004, 2014.

Zoogman, P., Liu, X., Suleiman, R. M., Pennington, W. F., Flittner, D. E., Al-Saadi, J. A., Hilton, B. B., Nicks, D. K., Newchurch, M. J., Carr, J. L., Janz, S. J., Andraschko, M. R., Arola, A., Baker, B. D., Canova, B. P., Chan Miller, C., Cohen, R. C., Davis, J. E., Dussault, M. E., Edwards, D. P., Fishman, J., Ghulam, A., Gonzalez Abad, G., Grutter, M., Herman, J. R., Houck, J., Jacob, D. J., Joiner, J., Kerridge, B. J., Kim, J., Krotkov, N. A., Lamsal, L., Li, C., Lindfors, A., Martin, R. V., McElroy, C. T., McLinden, C., Natraj, V., Neil, D. O., Nowlan, C. R., O'Sullivan, E. J., Palmer, P. I., Pierce, R. B., Pippin, M. R., Saiz-Lopez, A., Spurr, R. J. D., Szykman, J. J., Torres, O., Veefkind, J. P., Veihelmann, B., Wang, H., Wang, J., and Chance, K.: Tropospheric emissions: Monitoring of pollution (TEMPO), Journal of Quantitative Spectroscopy and Radiative Transfer, 186, 17–39, https://doi.org/10.1016/j.jqsrt.2016.05.008, 2017.

Zuromski, L. M., Bowling, D. R., Köhler, P., Frankenberg, C., Goulden, M. L., Blanken, P. D., and Lin, J. C.: Solar-Induced Fluorescence Detects Interannual Variation in Gross Primary Production of Coniferous Forests in the Western United States, Geophysical Research Letters, 45, 7184–7193, https://doi.org/10.1029/2018gl077906, 2018.